Master Thesis

The TU Wien Turbulent Water Channel: measurements and statistics

carried out for the purpose of obtaining the degree of Master of Science (MSc), submitted at TU Wien, Faculty of Mechanical and Industrial Engineering, by

Vlad Giurgiu

Mat.Nr.: 1229563

under the supervision of

Univ.Prof. Dipl.-Ing. Dr.-Ing. Alfredo Soldati

Institute of Fluid Mechanics and Heat Transfer, E322

Vienna, April 2021

I confirm, that going to press of this thesis needs the confirmation of the examination committee.

Affidavit

I declare in lieu of oath, that I wrote this thesis and performed the associated research myself, using only literature cited in this volume. If text passages from sources are used literally, they are marked as such.

I confirm that this work is original and has not been submitted elsewhere for any examination, nor is it currently under consideration for a thesis elsewhere.

I acknowledge that the submitted work will be checked electronically-technically using suitable and state-of-the-art means (plagiarism detection software). On the one hand, this ensures that the submitted work was prepared according to the high-quality standards within the applicable rules to ensure good scientific practice "Code of Conduct" at the TU Wien. On the other hand, a comparison with other student theses avoids violations of my personal copyright.

Vienna, April 2021_____

City and Date

Signature

Acknowledgments

I would like to thank my supervisor, Prof. Alfredo Soldati for the opportunity he gave me to start my career and to work alongside him and his team.

I am deeply grateful to my co-supervisor, Dr. Marco De Paoli for his continuous support, guidance, and patience. I thank him for the generosity with his time, for his friendship, and for being a role model to me. I thank him for the execution of the direct numerical simulations in turbulent channel and duct flow and for providing me with the results.

I also like to thank Dr. Mobin Alipour for carrying out the experiments in the duct and for providing me the data resulting.

I am thankful to Dr. Hadi Sichani for the execution of the direct numerical simulation in a turbulent channel and providing me with the results.

I thank my colleagues at the Institute of Fluid Mechanics and Heat Transfer for creating a welcoming and friendly atmosphere to work in.

Last, but not least I would like to thank my family and Dalmonia for their invaluable help and support. This thesis is dedicated to them.

Abstract

The statistical properties of a turbulent duct flow are investigated experimentally. Experiments are performed in the TU Wien Turbulent Water Channel at a shear Reynolds number of 370. A high-speed imaging system is used to record the flow and the velocity fields are obtained via three-dimensional particle tracking velocimetry (3D-PTV). Experimental results are first used to compute the first four moments of the velocity distribution and then compared against direct numerical simulations (DNS). It was found that in the duct, the statistics of all velocity components exhibit good agreement with those obtained from DNS. Slight overestimation of the main Reynolds stresses, particularly close to the wall, has been observed. Skewness and flatness of the stream-wise velocity were underestimated in the viscous sub-layer. Moreover, a new method is proposed to correct the misalignment of the measurement volume with respect to the actual flow direction. This method successfully reduced the average span-wise velocity. Finally, we analysed the effect of the width-to-height aspect ratio (AR) on the flow statistics. We analysed DNS of duct flows with $1 \leq AR \leq 8$ and we observed that, at a shear Reynolds number of 150, a duct with $AR \leq 8$ is not sufficient to reproduce the statistical properties observed in a turbulent channel flow ($AR = \infty$). These findings are significant because they provide evidence of the turbulence characteristics in the TU Wien Turbulent Water Channel.

Contents

List of Figures

List of Tables

1

Introduction

The aim of this study is to investigate the statistical properties of a water flow in a duct to certify that a statistically one-dimensional turbulent flow is present, i.e. averaged flow quantities only vary in the wall-normal direction. Thus the aim is to show that the lateral walls have no effect on the flow properties in the middle of the duct and that the statistical properties do not change in the stream-wise direction. This will serve as the foundation for other studies which will be carried out in the TU Wien Turbulent Water Channel.

The study of turbulent pipe and duct flows is done to investigate the characteristics of wall-bounded turbulent flow in general. The relative simplicity of the geometry and the ease of control of a duct flow facility are attractive for such studies. In particular the understanding of these flows is of significant importance in industrial processes. Predicting pressure losses, mixing behaviour, and heat transfer in fluid transport systems is key to designing machinery, plants, and pipelines. Moreover advancements in understanding these flows allow for control and optimisation. Industrial techniques derived from the study of turbulent duct and pipe flows are for example the injection of a copolymer solution (Warholic et al., 2001) or injection of a secondary immiscible fluid, like water in oil pipelines, to reduce pressure losses. Wall-bounded turbulent flow is also studied with the aim to understand interactions between particles of different types and shapes with the turbulent flow field. Applications range from paper-making (Lundell et al., 2011), to reducing contamination of bodies of water with micro plastics, and the formation of icy clouds which reflect the suns radiation back into space (Heymsfield, 1977).

The significance of turbulent wall-bounded flows is also evident from the rich history of experimental observations, numerical investigations, and analytical work done over the span of almost two centuries. The following is by no means a complete list of all such endeavours, but should serve the reader as an introduction to this vast field of experimental probing into duct flows. The reported Reynolds numbers are computed with the bulk velocity and full height of the channel. Investigations on the resistance against the

motion of fluids go back to Darcy (1857) and even sooner. In the well-known report of Reynolds (1883) the transition from laminar to turbulent flow in a glass pipe is observed and a fit for pressure losses is provided. Among the first reports on the mean flow at high Reynolds numbers lies the work of Nikuradse (1929). Reichardt (1938) extended the measurements on the velocity fluctuations in stream-wise and wall-normal directions. Measurements of the mean flow, the velocity fluctuations in span-wise and wall-normal direction in a high aspect ratio duct (12 : 1) and bulk Reynolds numbers $2.4 - 12.2 \times 10^4$, their cross-correlation, and mean shear were reported by Laufer (1948). Higher order statistics such as skewness, flatness and energy spectra were reported by Comte-Bellot (1963). The investigated range of Reynolds numbers was $11.4 - 46 \times 10^4$. Measurements in close proximity to the wall, well within the viscous sub-layer have been carefully carried out by Clark (1968) for Reynolds numbers $2 - 26 \times 10^4$ (based on the center-line velocity and the full height) in a wind tunnel of aspect ratio 12 : 1 and thus the wall shear could be computed. Mean velocity and their fluctuations and spectra for all components were reported. Patel and Head (1969) note the difficulty in precisely defining what "fully turbulent flow" means: if it's defined based on a particular skin-friction law, a certain mean velocity profile, known as the law of the wall, or on the continuous chaotic motion, i.e. no intermittency. They investigated pipe and duct flow with Reynolds numbers $0.1 - 1 \times 10^4$ and concluded that depending on the chosen criterion different critical Reynolds number, upwards of which the flow is considered fully turbulent can be found. Later Wallace et al. (1972) focused on the production of Reynolds stresses and associated the sign of the cross-correlation between stream-wise and wall-normal velocity fluctuations with different classes of interactions with the wall, events, such as sweep and ejection. Hussain and Reynolds (1975) used a duct with an aspect ratio of 18 : 1. In order to reduce the influence of the rearrangement of the flow at the entrance on the measurements a much longer development length, i.e. the distance from the entrance to the measuring station, to half-height ratio (450) than Laufer (1948), Comte-Bellot (1963), and Clark (1968) with 86, 122, and 120, respectively. The facility was used to test if such a duct can produce a good approximation of a fully developed, statistically one-dimensional turbulent flow. They studied flows at three different Reynolds numbers in the range $2.8 - 6.6 \times 10^4$ and concluded based on the duct center line stream-wise velocity profile over the span-wise direction, that the flow was fully developed and one-dimensional for the central 70% of the duct span. Later Dean and Bradshaw (1976) studied the interaction between shear layers in a duct-flow of aspect ratio 12 : 1 at a Reynolds number of 10×10^4. One wall was heated in order to distinguish between the 'hot' and 'cold' boundary layers forming at the entrance and to investigate their interplay after meeting in the central region. They concluded that such a flow is considered fully turbulent after a steady rate of big scale motion between the two regions and of small scale mixing is achieved. Using hot-

film probes Kreplin and Eckelmann (1979) measured all three components of the velocity fluctuation and two components of wall shear stress fluctuation. They reported root-mean-square values, skewness, flatness profiles over the distance from the wall, and probability density functions. They noted the non-Gaussian nature of such wall bounded turbulent flows, but also the necessity of investigation of probe interference on the measurements. Johansson and Alfredsson (1982) also used hot-film probes to measure the stream-wise velocity at three Reynolds numbers (based on the center-line velocity): 1.38, 3.46, and 4.89×10^4 and reported the first four statistical moments. They used a short-time variance technique, called VITA, to detect structures and to correlate them to skewness and flatness factors. Wei and Willmarth (1989) investigated the Reynolds number dependence of velocity statistics. They measured the stream-wise and wall-normal velocity components using a Laser Doppler Anemometer at high acquisition rates and resolution for a Reynolds number (based on the center-line velocity) range of $0.6 - 8 \times 10^4$ and concluded that fluctuating quantities such as Reynolds stresses and power spectra are Reynolds number dependent when scaled by inner variables. They also noted the existence of a 'geometric effect' where the inner regions at opposing duct walls interact, in particular for their lowest studied Reynolds number flow. This interplay was less evident for a higher Reynolds number. The Reynolds number dependency of the Reynolds stresses scaled by wall variables was also confirmed by Antonia et al. (1992) through experiment and direct numerical simulation. They also confirmed the increasing penetration depth and frequency of fluid from one wall to the other with decreasing Reynolds numbers, but found no evidence of significant impact on the Reynolds stresses in the inner region of the opposite wall. In the endeavour to define if a duct flow is fully turbulent, Lien et al. (2004) studied the mean stream-wise velocity profiles over the distance from the wall scaled by inner variables at different distances from the entrance. The measurements were carried out at three different Reynolds number: 4, 10.5, and 18.5×10^4 and the authors concluded that a minimum length to half-height ratio of 260 is required for full development. They also noted that a thorough investigation with the aim of defining development should also include other turbulence quantities. Li et al. (2005) investigated the effect of a surfactant solution on the turbulence statistics and structures. They used a particle image velocimetry system in a duct of aspect ratio 12.5. The solution showed a drag-reducing effect. Cai et al. (2009) also found a drag-reduction effect of the cetyltrimethyl ammonium chloride solution of 70% in comparison with pure water flow. The investigated Reynolds number was 2.5×10^4. The measurement of the skin-friction coefficient by two different methods, namely oil film interferometry and stream-wise mean pressure gradient was carried out and compared by Zanoun et al. (2009b). The experiments were done in a duct of width-to-height aspect ratio of 12 : 1 at Reynolds numbers up to 2.4×10^5. Both types of measurements agreed well with the fit proposed by Dean (1978). Us-

ing center-line turbulence statistics up to forth order Zanoun et al. (2009a) study the development and transition behaviour of flows in a pipe and a duct using a hot-wire anemometer and a laser doppler anemometry technique. They found that the development length and transition Reynolds number are dependent on the flow conditions at the entry. Ng et al. (2011) provide average stream-wise velocity and turbulent intensity profiles for pipe and duct flows at shear Reynolds number of $10^3 \leq Re_\tau \leq 3 \times 10^3$. These were obtained experimentally with hot-wire anemometry. Further experimental evidence of turbulent duct flows is provided by Schultz and Flack (2013). The aspect ratio of the facility was 8. The investigated shear Reynolds number range is $10^3 \leq Re_\tau \leq 6 \times 10^3$. They reported the friction factors, average stream-wise velocity profiles, and shear and normal Reynolds stresses profiles. The measurements agreed well with the compared results of direct numerical simulations. More comparisons with DNS found during the literature review are given in Sec. 4.1.

A summary of recent investigations carried out in turbulent duct flow is given in Table. 1.1. They are sorted by the width-to-height aspect ratio of the duct - an important measure for the statistical two-dimensionality of the flow at the centre plane in span-wise direction. The studied bulk Reynolds number Re computed with the half-height is shown. The ratio of development length to duct height and the height are reported. Moreover the type of the investigation is shown: experimental and/or direct numerical simulation. The ability to resolve the flow in time and the dimension of the measurement volume: 0 for point-wise, 2 for planar, and 3 for volumetric measurements are reported. Lastly the velocimetry technique and the working fluid are given. It is evident that the TU Wien Turbulent Water Channel is not especially wide, long, and can't generate higher Reynolds numbers than other facilities, but it stands out because of its state-of-the-art measurement technique - a high speed three dimensional three component particle tracking velocimetry, and the working fluid - water. Thus one is able to investigate the three dimensional and time-resolved motion of a wide spectrum of particle interacting with a turbulent flow field: from spherical and rigid to anisotropic and deformable such as fibres, from non-inertial and neutrally buoyant to inertial and buoyant particles. It was designed and built for this purpose.

One of the main observations which were made during the literature review is that there is no consensus on how long or wide (see also Chapter 3) a duct should be in general for the turbulent flow to be considered fully developed and statistically one-dimensional, i.e. the statistical quantities are only a function of the wall-normal direction. This work does not aim to make such general statements, as it was observed also by other authors (Hoyas and Jiménez, 2006) that experimental results show a clustering behaviour by facility rather that physical parameters such as the Reynolds number. Thus this study aims to provide evidence of the statistical turbulence properties in this facility and compare it to direct numerical simulations.

Reference	AR	Re	$L/(2h)$	$2h$	Type	Time res.	Dim.	Velocimetry	Fluid
	[-]	10^4	[-]	[mm]					
Kitagawa et al. (2005)	6.67	4.12	200	15	Exp.	No	2	PTV, LIF, SIT	W. + A.
Schultz and Flack (2013)	8	$0.5-15$	124	25	Exp.	No	0	PT, LDV	W.
Mamori et al. (2019)	10	0.225	166.25	20	Exp./DNS	Yes	2	DPS. PIV	A.
So et al. (2002)	10	$0.0675-0.41$	50	40	Exp.	Yes	0	LDV	W. + A.
Murai et al. (2006)	10	1	400	10	Exp.	Yes	2	PTV	W. + A.
Present study	10	up to 3	110	80	Exp./ DNS	Yes	3	3D PTV	W.
Moroni and Cenedese (2005)	11	$0.2-0.485$ (c)	80	20	Exp.	No	2	PIV, PTV, FT	W.
Lien et al. (2004)	11.7	$2-9.25$	205	100	Exp.	No	0	PST, PT	A.
Wei and Willmarth (1989)	11.85	$0.3-4$ (c)	86	25.72	Exp.	Yes	0	PT, LDA	W.
Warholic et al. (2001)	12	$1.88-2.03$	NA	50.8	Exp.	No	2	PIV	W., poly.
Li et al. (2005)	12.5	$0.27-1.82$	175	40	Exp.	No	2	PIV	W., surf.
Antonia et al. (1992)	18	$0.33-2.15$ (c)	320	42	Exp./ DNS	Yes	0	HWA	A.
Schaefer et al. (2011)	20	$0.33-3.3$	115	100	Exp.	Yes	3	PIV	A.
Recktenwald et al. (2007)	10, 25, 50	0.285	80	20	Exp./ DNS	No	2	PIV	W.
Vinuesa et al. (2014)	12.8 - 48	$0.25-2$ (c)	96 - 576	6.35 - 15.88	Exp./ DNS	No	0	PT, OFI	A.

TABLE 1.1 – Summary of recent experimental investigations of a turbulent duct flow. The works are sorted by the duct aspect ratio (AR). Re is the bulk Reynolds number computed with the integral length, i.e. half-height between the walls with the largest span. The abbreviation (c) denotes that the Reynolds number was computed with the center-line velocity. The ratio between the length from the flow entrance into the duct to the test section to twice the integral length ($L/(2 \times h)$) is also shown. The type: experiment and/or direct numerical simulation is also reported. Facilities showing the capacity to resolve the velocity field in time (abbreviation: Time res.) are also noted. The interrogation space is also reported (Dim.): 0 - point-wise, 2 - planar, and 3 - volumetric measurements. Velocimetry techniques are reported and abbreviated as follows: particle tracking velocimetry (PTV), laser-induced fluorescence (LIF), shadow image technique (SIT), pressure taps (PT), laser Doppler velocimetry (LDV), dual plane stereo particle image velocimetry (DPS. PIV), three-dimensional particle tracking velocimetry (3D PTV), feature tracking (FT), Pitot-static tubes (PST), hot wire anemometry (HWA), and oil-film interferometry (OFI). Lastly, the working fluid is reported. The abbreviations w., a., poly., surf. mean water, air, polymere solution, and surfactants respectively.

2

Methodology

The three-dimensional velocity field of a water flow in the TU Wien Turbulent Water Channel is measured with the aim of characterising the turbulent flow based on the first four moments of the velocity components. This chapter will introduce the facility's main features, imaging equipment and parameters, and flow quantities. Moreover the statistical approach is introduced here.

2.1   Experimental setup

The TU Wien Turbulent Water Channel is the experimental facility and subject of this study. It is a water channel with a length of 10 m and an inner cross-section of 800×80 mm^2 (width $\times$ $2h$, where h is the ducts half-height). The walls are 15 mm thick and are produced of Polymethyl methacrylate (PMMA), a transparent thermoplastic. The duct is made of an assembly of five 2 m long sections. The upper covers of each section are removable so that the facility can reproduce both an open and closed duct configuration. The present investigation is reserved only to the closed configuration. A schematic of the set-up is shown in Fig. 2.1 in panel a). The working fluid is still water and is driven by gravity from the upstream reservoir through the entire length of the duct, passing the test section at ≈ 8.5 m from the entrance. It returns to the downstream reservoir from where it is pumped by a centrifugal pump back to the upstream reservoir.

The maximum pump flow rate is ≈ 147 m^3 h^{-1} and the flow rate is measured by an electromagnetic flow-meter (Proline Promag 10D). Before and after each experiment the water temperature is measured by an analog mercury thermometer and for the experiments presented here it measured $15\,°\mathrm{C}$.

The cameras and laser are placed on rubber spacers. The laser cooler is mounted on a damping platform to reduce the transmission of vibrations to the sensitive laser and camera system. Moreover the centrifugal pump is also placed on rubber spacers for the same reason.
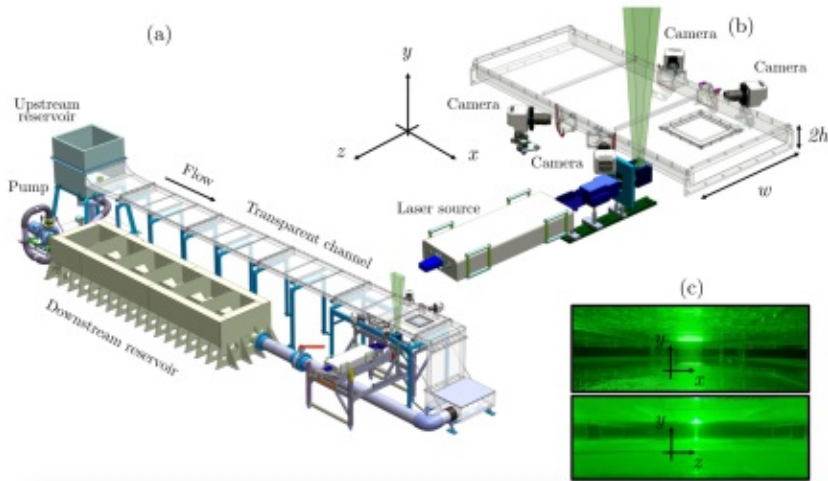
FIGURE 2.1 – The schematic of the TU Wien Turbulent Water Channel is shown. In panel (a) the general layout and main components are shown: a rectangular duct of aspect ratio 10, two reservoirs at ambient pressure, a centrifugal pump, and a test section located 8.5 m downstream from the entrance. Panel (b) shows a close-up view of the test section where four high-speed cameras record the motion of tracers in the volume illuminated by the laser. The laboratory reference system is also shown as x, y, and z - stream-wise, wall-normal, and span-wise directions respectively. Panel (c) shows the illuminated volume in stream-wise (upper panel) and in span-wise directions (lower panel). Courtesy of Alipour et al. (2021).

The illumination and velocimetry equipment are located at 8.5 m (equivalent to $\approx 210h$) from the entrance. The measurement and illumination volume measures $53.4 \times 53.4 \times 14$ mm^3 in stream-wise, wall-normal, and span-wise direction respectively and is situated in the middle of the duct span-wise. Fig. 2.1 panel b) shows a close-up view of the test section. The illumination of the volume is provided by a double cavity laser: Litron LD60-532 PIV (527 nm). The set energy per pulse was 24 mJ. The images required for velocimetry were recorded by four Phantom VEO 340L cameras (sensor resolution 2560×1600 pixels with a pixel size of 10×10 µm^2). The side and front views of the illuminated volume are shown in Fig. 2.1 panel c). On both sides of the duct there are two cameras placed in linear configuration inclined at angles of 30° and 35° from the span-wise direction. Furthermore four prisms filled with water have been placed in the optical path of the camera lenses. They are also equipped with Scheimpflug adaptors and with lenses with a focal length of 100 mm. Another piece of equipment required for the laboratory coordinate system mapping on the recorded images is a calibration target (size 58×58mm^2).

The recordings were done at a frequency of 1 kHz and at a cropped resolution of 1280×1280. The aperture was set at $f/22$. The magnification was 0.24. Thus the resulting resolution was 0.04166 mm/pixel. The particle per

pixel density (ppp) was 0.02 for tracers with a 20 μm diameter. The tracers are neutrally buoyant and non-inertial. The Stokes number is considered here as the ratio between the tracer relaxation time ($d^2/18\nu$, where d is the tracer diameter) and the viscous time scale (τ) and is $\approx 2 \times 10^{-3}$. All the required processing for the three-dimensional particle tracking velocimetry (3D-PTV) was done in the software DAVIS (La Vision G.m.b.H.). Granular details about the image processing parameters are found in Alipour et al. (2021).

For these experiments a constant flow-rate of $42 \, \mathrm{m^3 \, h^{-1}}$ was chosen. This is equivalent to a bulk velocity of $u_b = 0.183 \, \mathrm{m \, s^{-1}}$. The kinematic viscosity of water at $15 \, °\mathrm{C}$ is $\nu = 1.139 \times 10^{-6} \, \mathrm{m^2 \, s^{-1}}$ (Kind and Martin, 2013). Thus the bulk Reynolds number computed with the full height of the channel is $Re_b = 2hu_b/\nu = 12800$. The shear Reynolds number is estimated to be $Re_\tau \approx 370$ (The estimation $Re_\tau \approx 0.09Re_b^{0.88}$ (Pope, 2001) was used here). The pressure drop is not measured because it is too small ($\approx 3 \times 10^{-2}$ mbar m^{-1}). The approximate friction velocity is thus $u_\tau = \nu Re_\tau/h \approx 0.0105 \, \mathrm{m \, s^{-1}}$. The viscous length scale is $l_\tau = h/Re_\tau \approx 108 \, \mu\mathrm{m}$ and the viscous time scale is $\tau = \nu/u_\tau^2 \approx 10 \, \mathrm{ms}$. The Kolmogorov length scale in the middle of the duct is $\eta \approx 377 \, \mu\mathrm{m}$ (the estimation $\eta = l_\tau(\kappa y^+)^{0.25}$ (Pope, 2001) was used here, where $\kappa = 0.4$). For reference, the Kolmogorov length at $y^+ = 1$ is $\eta \approx 86 \, \mu\mathrm{m}$.

2.2 Statistical approach

The equations describing the motion of a single phase incompressible fluid flow with constant physical properties are the continuity of mass and the momentum balance, known as Navier-Stokes equations (here the Einstein summation notation is used):

$$\partial_j u_j = 0 \ , \tag{2.1}$$

$$\partial_t u_i + u_j \partial_j u_i = -\frac{1}{\rho}\partial_i p + \nu\partial_j^2 u_i \ , \tag{2.2}$$

where u_i are the three velocity components, ρ is the fluid density, p is the pressure, and ν is the kinematic viscosity. Note that in the rest of the document u_1, u_2, and u_3 are referred to as u, v, and w, respectively.

If one considers a turbulent flow as a stochastic phenomenon due to its high sensitivity to initial and boundary conditions and the inherent imperfections in such conditions in the real world, then one may decompose the velocity and pressure fields in a mean value ($\langle\cdot\rangle$), i.e. the probability weighted average of all possible values ($\cdot$), and a fluctuating part ($\cdot'$) around this mean, also known as the *Reynolds decomposition* (Pope, 2001):

$$u_i = \langle u_i \rangle + u_i' \ , \ p = \langle p \rangle + p' \ .$$

Taking into account the property that the mean of the fluctuations is zero ($\langle \cdot' \rangle = 0$) and using the decomposition in Eq. (2.1) and Eq. (2.2) one finds the following mean equations:

$$\partial_j \langle u_j \rangle = 0 \ , \tag{2.3}$$

$$\partial_t \langle u_i \rangle + \langle u_j \rangle \partial_j \langle u_i \rangle = -\frac{1}{\rho} \partial_i \langle p \rangle + \nu \partial_j^2 \langle u_i \rangle - \langle u_j' \partial_j u_i' \rangle \ . \tag{2.4}$$

Multiplying Eq. (2.4) by the density ρ and using the property that the fluctuations field is also divergence free ($\partial_j \langle u_j' \rangle = 0$) one can cast the following equation:

$$\rho \left(\partial_t \langle u_i \rangle + \langle u_j \rangle \partial_j \langle u_i \rangle \right) = -\partial_i \langle p \rangle + \partial_j \left\{ \mu \left[\partial_j \langle u_i \rangle + \partial_i \langle u_j \rangle \right] - \rho \langle u_j' u_i' \rangle \right\} \tag{2.5}$$

The components of the term $\rho \langle u_j' u_i' \rangle$ are in form similar to the viscous stresses ($\mu \left[\partial_j \langle u_i \rangle + \partial_i \langle u_j \rangle \right]$) and act similar to an enhanced viscosity, but they are a direct consequence of the non-linear interaction of the velocity field ($u_j \partial_j u_i$). Even for a statistically stationary flow, they are a function of space. These single-point correlations are from this point-of-view dissimilar to viscous dissipation, but their formal similarity has been exploited many times in the search for understanding and computing turbulent flows. Note that only the deviatoric part $\langle u_i' u_j' \rangle_{i \neq j}$ contributes to the transfer of mean momentum, while isotropic ones $\langle u_i' u_j' \rangle_{i=j}$ act as a modified pressure and represent the variance of the velocity distribution (Pope, 2001). Thus they quantify the spread of the fluctuating values around the average. Note that throughout this document it will be refer to $\langle u_j' u_i' \rangle$ as *Reynolds stresses*, even though formally they are not stresses.

As any investigation must be limited to a non-infinite number of experiments every mean ($\langle \cdot \rangle$) reported here is approximated by an ensemble average ($\langle \cdot \rangle_N$), an average over independent experiments. Furthermore the assumption of ergodicity is made, motivated by the statistical stationary and in stream-wise and span-wise homogeneous flow, under which the average in time ($\langle \cdot \rangle_t$) and in space ($\langle \cdot \rangle_{x,z}$) are equivalent with the ensemble average. Note that for this reason only the notation $\langle \cdot \rangle$ will be used and the mean quantities will be approximated by:

$$\langle q \rangle \approx \frac{1}{N_x N_z N_t} \sum_{k=1}^{N_x} \sum_{l=1}^{N_z} \sum_{m=1}^{N_t} q_{k,l,m} \ , \tag{2.6}$$

where q can be the stream-wise, wall-normal, span-wise velocity u, v, and w respectively, the velocity fluctuations squared $u'u'$, $v'v'$, and $w'w'$ respectively, or third and forth order velocity fluctuations u'^3, v'^3, w'^3, and u'^4, v'^4, w'^4 respectively. Thus the skewness s and flatness f have been chosen

for third and forth order statistics (shown here only for the stream-wise velocity u, but the same holds for the other components):

$$s_u = \langle u'^3 \rangle / \langle u'^2 \rangle^{3/2} \tag{2.7}$$

$$f_u = \langle u'^4 \rangle / \langle u'^2 \rangle^2 \tag{2.8}$$

The skewness factor quantifies the asymmetry in the probability density function. Note that for a Gaussian random process the skewness is zero ($s = 0$). The flatness factor, known also as kurtosis, quantifies the likelihood of extreme events, both with high and low velocity fluctuations, of occurring. Note that for a normal distribution the flatness is three ($f = 3$).

3

Effect of aspect ratio on statistics

The geometry of a duct, i.e. a long pipe with rectangular cross-section, seems to be the most simple one to conduct experiments in. Nonetheless many experimenters and numerical investigators would prefer an even simpler geometry - a flow between two infinitely extended plates, i.e. a channel. This provides ideal conditions to study a statistically one-dimensional problem. This impossible to realize situation is approximated in a numerical investigation by periodic boundary conditions at the lateral walls, i.e. in the span-wise direction. The experimentalist approximates such a flow by using a high aspect ratio of width-to-height of the duct in the hope to reduce the influence of the side walls on the flow in the middle. The debate about the minimum required aspect ratio for on average one-dimensionality has been going on more than half a century. After consulting 42 works and reviewing 27 of them on turbulent duct flow, Dean (1978) concluded based on the invariance of bulk parameters such as skin friction factor at different aspect ratios over 7 : 1 that this threshold is the minimum recommended. Zanoun et al. (2003) used a duct of aspect ratio 12 : 1 and based on the comparison between the friction factor measured from the pressure drop and the one from the wall shear stress considered the flow sufficiently statistically one-dimensional. More recently Vinuesa et al. (2014) recommended an aspect ratio of at least 24 : 1. They measured the wall shear stress with oil-film interferometry and the centre line velocity with Pitot tubes. They argued that these are the most suitable quantities to scale the friction factor with because they represent the actual shear-stress, not an average one, and the development state of the flow. They presented their results in terms of the center line velocity scaled by the shear velocity over the shear Reynold number. Higher aspect ratios than 24 : 1 did not have any effect on this scaling, while it was obvious that lower ones did show a shift of this function. Moreover they argued that a span-wise periodic DNS channel is a different system from a wide experimental duct based on the different scaling of the two systems. Their argument is physically well

Syst.	Re_τ	Re_b	Grid	Domain size	AR	Avg. int.
			$N_x \times N_y \times N_z$	$L_x \times L_y \times L_z$		τ
channel	180	5640	$512 \times 256 \times 144$	$12h \times 6h \times 2h$	∞	16000
duct	150	4410	$256 \times 128 \times 128$	$5h \times 2h \times 2h$	1	5000
duct	150	4410	$256 \times 128 \times 256$	$5h \times 2h \times 4h$	2	5000
duct	150	4410	$256 \times 128 \times 512$	$5h \times 2h \times 8h$	4	5000
duct	150	4410	$256 \times 128 \times 1024$	$5h \times 2h \times 16h$	8	5000

TABLE 3.1 – Table summarizing the details of the performed DNS in channel and duct flow. The shear Reynolds number Re_τ, computed with the friction velocity and the half-height and the bulk Reynolds number Re_b, computed with the bulk velocity and full height of the duct are listed. The grids have uniform spacing and number of grid points in stream-wise (x), wall-normal (y), and span-wise (z) are reported. The domain size is listed. The half-height is h. The aspect ratio of the geometry (AR) is also reported. The averaging interval for the statistical quantities is listed in terms of the viscous time scale (τ) is given. The direct numerical simulations were executed by De Paoli (2021) with the *CaNS* code.

motivated. However most recently Vinuesa et al. (2018) investigated the extend of secondary flow generated by the lateral walls stretching towards the center. They compared direct numerical simulations of ducts with aspect ratios between 1 and 14.4 with that of a span-wise periodic channel at shear Reynolds number of 180. They concluded that experimental ducts of aspect ratio larger than 10 can be used to compare with span-wise periodic channel obtained by DNS, because they exhibit similar behaviours. Moreover they point out that a previous study (Vinuesa et al. (2014)) may have suffered from experimental uncertainties which led to the recommendation of larger aspect ratios.

In the light of these recent developments the aim of this work is more firmly motivated. The aim is to certify that the duct flow in the TU Wien Turbulent Water Channel is for the intents and purposes it was build for, statistically one-dimensional, i.e. the statistical quantities in the center (span-wise) only vary in the wall-normal direction. Thus an investigation of the effects of aspect ratio on the turbulent flow by comparing statistics up to forth order is proposed.

3.1 Direct numerical simulation of channel and duct flow

Direct numerical simulations (DNS) were used to compare a channel to a duct flow based on the first four moments of the stream-wise velocity component. The channel simulation has no-slip and no-penetration boundaries at the top and bottom walls and periodic boundary conditions at the lateral walls and in stream-wise direction. This was executed at a shear Reynolds number of 180. The duct flow simulation has no-slip and no-penetration
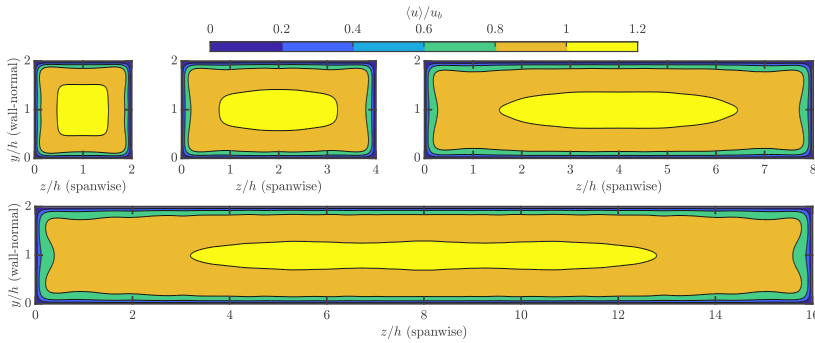
FIGURE 3.1 – A qualitative picture of the stream-wise velocity averaged over time and stream-wise direction for flow in different aspect ratio ducts at bulk Reynolds number $Re = 4410$ - computed with the full height. This is equivalent to $Re_\tau \approx 150$. These are cross-sections. The bulk velocity is u_b. Different width-to-height aspect ratios 1, 2, 4, and 8 are shown in the order from left to right and from top to bottom. These results were obtained by direct numerical simulation (Courtesy of De Paoli (2021)).

lateral, upper, and lower boundaries with periodic conditions in stream-wise direction and was carried out at $Re_\tau \approx 150$ for different width-to-height aspect ratios of $AR = 1$, 2, 4, and 8. Both have been executed by De Paoli (2021) with the open-source `FORTRAN` code $CaNS$ (Canonical Navier-Stokes), a finite-difference pseudo-spectral solver (Costa, 2018). Details, such as number of grid points, domain size, aspect ratio, and temporal averaging interval are summarized in Table. 3.1.

The Fig. 3.1 shows the time and stream-wise averaged stream-wise velocity scaled by the bulk velocity in a cross-section through all the simulated ducts. All the investigated aspect ratios in duct flow are shown. It is observable that for all the ducts the highest average velocity gradients are situated close to the walls. Moreover there is an observable evolution of the averaged stream-wise velocity at the half-height with increasing aspect ratio. The region of high velocity becomes thinner and is stretched. Based on these qualitative results an argument can be made that the duct of an aspect ratio of 8 (panel d) of Fig. 3.1) is statistically one-dimensional for a region spanning from around $5h$ to about $11h$.

The Fig. 3.2 shows the root-mean-square of the stream-wise velocity scaled by the bulk velocity in a cross-section through all the simulated ducts. The results were averaged over time and the stream-wise direction. All the investigated aspect ratios in duct flow are shown. It is evident that the fluctuations are for all simulations concentrated near the walls. Moreover one can appreciate that there is an evolution of the distribution of the fluctuations with increasing aspect ratio. Near the upper and lower walls the distribution gets squeezed and stretched, while in the middle the region of low fluctuations gets thicker. Based on these qualitative results an aspect ratio of 8 (bottom panel of Fig. 3.2) is statistically one-dimensional in
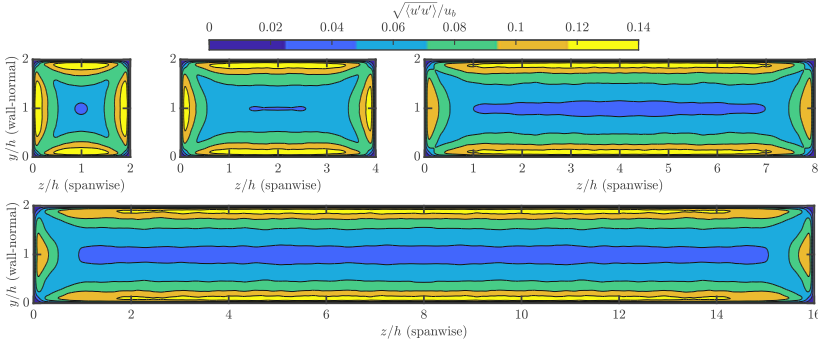
FIGURE 3.2 – A qualitative picture of the root-mean-square of the stream-wise velocity fluctuations averaged over time and stream-wise direction for flow in different aspect ratio ducts at bulk Reynolds number $Re = 4410$ - computed with the full height. This is equivalent to $Re_\tau \approx 150$. These are cross-sections. The bulk velocity is u_b. Different width-to-height aspect ratios 1, 2, 4, and 8 are shown in the order from left to right and from top to bottom. These results were obtained by direct numerical simulation (Courtesy of De Paoli (2021)).

the center of the duct because the distribution of the fluctuations does not change for most of the width - from around $3h$ to around $11h$. The statistical properties were invariant of time, as the simulated time was enough for achieving a statistically stationary process which was also invariant of the stream-wise direction.

3.2   Quantifying differences between duct and channel flow

In order to quantify these results a classical statistical approach has been used (as described in Sec. 2.2). Fig. 3.3 shows profiles of the first four moments of the stream-wise velocity at the center-plane in span-wise direction for all investigated ducts and are compared with the span-wise periodic channel. Looking at panel a) there are small differences observable between the profiles of the ducts with different aspect ratios and the channel profiles. They are not only different at the center-line, but also in the region $10 \leq y^+ \leq 75$. Observing the inset, it is clear that the duct of $AR = 8$ is closest at the center line to the channel profile. When moving closer to the wall (below $y^+ = 120$) the profiles show a different behaviour from the channel, because the Reynolds number does not match. The duct simulations were carried out in such a way that the pressure gradient was controlled so that a fixed bulk Reynolds number was achieved for the ducts (Costa, 2018). This does not ensure a fixed shear Reynolds number for different aspect ratio ducts. Turning our attention to the variance in panel b) of the same figure, a similar observation can be made: the higher the aspect ratio,
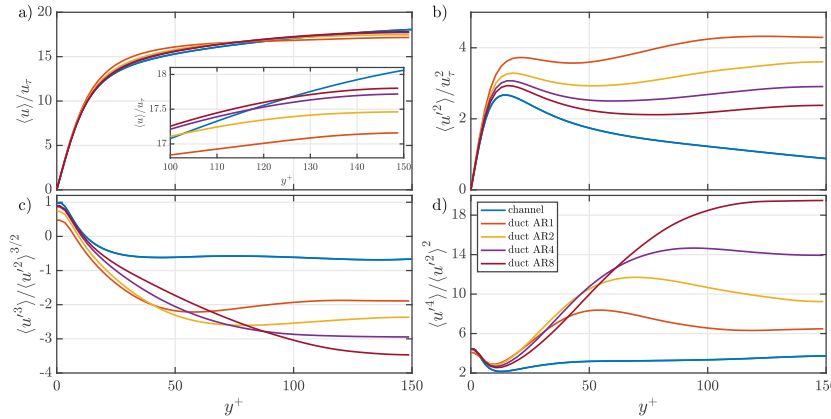
FIGURE 3.3 – A comparison of ducts with different aspect ratios based on the first four moments of stream-wise velocity is shown. The bulk Reynolds number $Re = 4410$ - computed with the half-height. This is equivalent to $Re_\tau \approx 150$. Width-to-height aspect ratios 1 (orange line), 2 (yellow line), 4 (violet line), and 8 (red line) are compared. The results from DNS of a channel flow at $Re_\tau = 180$ (blue line) are added. Panel a) and panel b) show the average span-wise velocity and average span-wise Reynolds normal-stress profile respectively over the wall-normal direction scaled by inner variables. Panel c) shows the skewness and panel d) shows the flatness of the span-wise velocity over the wall-normal direction. The abscissa of panel c) and d) apply to panel a) and d) respectively. These results were obtained by direct numerical simulation (Courtesy of De Paoli (2021)).

the closer the profile of the duct to that of the channel. The proximity to the walls generates higher fluctuations throughout the whole duct height. It is evident that an aspect ratio of 8 is at this shear Reynolds number not sufficient for approximating the statistical behaviour of a channel flow. Moreover the profile of a channel at $Re_\tau = 150$ would lie below the blue line (that of the current channel DNS at $Re_\tau = 180$). From this perspective even the high aspect ratio duct ($AR = 8$) overestimates the Reynolds stresses at the center-line by at least a factor of 2. This difference becomes smaller closer to the wall. The profiles of skewness in panel c) and flatness in panel d) show a reversed situation. The lower the duct aspect ratio the closer are the profiles of the duct to that of the channel. The skewness profiles in the ducts differ by a factor of 3 up to 5 from the one of the channel at the center. The flatness profiles of the $AR = 8$ duct differs by a factor of almost 5 from the channel at the center-line. The lower aspect ratio ducts are closer to the reference, but the closest result, that of $AR = 1$ is still overestimated by a factor of almost 2 at the center-line. Closer to the wall, e.g. at $y^+ = 50$ even larger differences are observed. Note that a Gaussian process would have a skewness of 0 and a flatness of 3.

In summary, at a bulk Reynolds number $Re = 4410$ (corresponding to $Re_\tau \approx 150$) neither of the ducts approximate the statistical behaviour of the channel DNS, not even the highest investigated aspect ratio of 8.

3.3   Flow structures close to the wall

In a wide range of industrial applications and environmental problems, suspensions of non-spherical particles, e.g. fibres are transported through different geometries at high velocities. These are turbulent wall-bounded flows and are characterised among others by high shear rates. Previous experimental and numerical studies have shown that, in such flows, fibres tend to agglomerate into stream-wise streaks in close proximity to the walls of the geometry (Håkansson et al., 2013). This is of significance in industrial processes such as paper making, because a non-uniform particle distribution results in lower quality products. In order to understand how particles interact with a turbulent wall-bounded flow, well resolved measurements of the strength of the tendency for the particles to agglomerate into streaks (Håkansson et al., 2013) are required. Aiming to make reliable comparisons between different system and geometry configurations, e.g. experiments compared to direct numerical simulations, or wide versus narrow channels, the streak-like structures should be carefully considered and precisely characterised. In low Reynolds number flows, the width and number of streaks observed is sensitive to the channel width. Thus the aspect ratio of the duct geometry is significant and has to be taken into account.
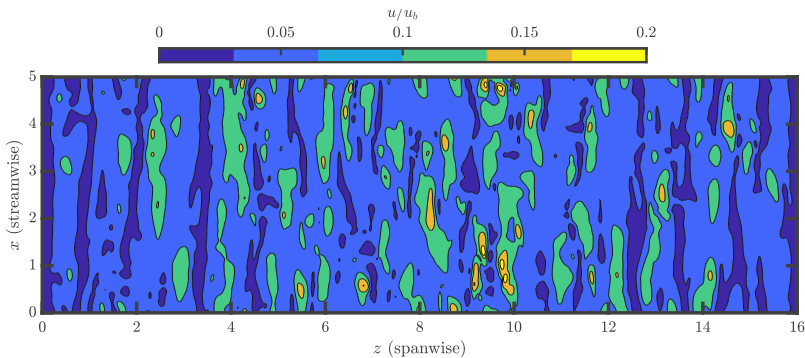
FIGURE 3.4 – A qualitative picture of the stream-wise velocity close to the wall at $y^+ = 2.4$ in a duct with aspect ratio 8 (DNS) is shown. The bulk Reynolds number is $Re = 4410$ - computed with the full height. This is equivalent to $Re_\tau \approx 150$. The bulk velocity is u_b. (Courtesy of De Paoli (2021)).

A qualitative picture of the instantaneous stream-wise velocity in close proximity to the bottom wall of a turbulent duct flow is provided in Fig. 3.4. The width-to-height aspect ratio is 8 and the results have been obtained by direct numerical simulation with the *CaNS* code. Streak-like structures of high and low velocities are observable. Similar measurements, in a region close to the wall are also possible and will be carried out in the TU Wien Turbulent Water Channel with the aim of investigating the interaction between these flow features and a wide range of particle types and shapes.

4

Results

4.1 Comparison with DNS

Statistical one-dimensionality of a turbulent flow means that the statistical properties, i.e. moments such as average, variance etc., are invariant to translations in two directions. If a turbulent flow field is statistically stationary and bound between two parallel walls with periodic boundary conditions in spanwise and streamwise directions, it is considered one-dimensional because the statistical properties do not change in span-wise and stream-wise direction as if the domain is infinitely extended. Such an investigation can only be carried out by numerical simulation and this geometry is named a channel. Experimental facilities, such as the TU Wien Turbulent Water Channel have to confine themselves to a limited domain. Thus a wide and long duct, i.e. a pipe with rectangular cross-section, is chosen. As was found in Chapter 3, the lateral walls have at low Reynolds numbers an influence on the statistical properties of the flow also in the middle of the duct (spanwise centerline). Increasing the width of the duct with respect to its height and the Reynolds number this influence of the lateral walls should decrease, because they are further from the middle in terms of the outer scales of the flow, but also in terms of inner scales. As a result this chapter is dedicated to the comparison between the statistical flow properties at the span-wise mid plane of the duct facility at the Vienna University of Technology with the channel DNS. Agreement between these two results are regarded as evidence for the low or non-existent influence of the lateral walls on the center, but also for the statistical invariance in the stream-wise direction.

The following list of comparisons between results from measurements in ducts and from direct numerical simulations in channel shows the popularity of such a procedure. On the one hand experimental results suffer from the intrinsic nature of the uncertainty of measurement and on the other hand simulations are based on multiple assumptions. Finding a good agreement between measurements and simulations one gains more confidence in the results, as this means that they are independent on the method of inquiry.

This principle is central to this chapter. The first numerical investigation of a channel flow where all turbulence scales were resolved has been carried out by Kim et al. (1987) at a Shear-Reynolds number of $Re_\tau = 190$ based on the half-channel height. They compared their results with experimental studies such as that of Kreplin and Eckelmann (1979) to confirm the independence of results from the investigation method, numerical or experimental. Comparisons between a span-wise and stream-wise periodic numerical channel and various experiments in pipes, ducts, and boundary layers were reported by Hoyas and Jiménez (2006). Average stream-wise velocity and Reynolds stresses have been compared for a rotating duct and numerical channel by Recktenwald et al. (2007) for different rotation rates. Monty and Chong (2009) compared a turbulent duct flow at $Re_\tau \approx 1000$ with a span-wise periodic channel DNS and found good agreement in the average velocity, normal stream-wise Reynolds stresses and energy spectra between the two. Turbulent channel flow was also compared to a duct flow with aspect ratio 20 by Schaefer et al. (2011) in terms of average velocities and root-mean-square and probability density functions of the fluctuations. Experimental evidence on the turbulence statistics were also provided and compared to DNS by Schultz and Flack (2013).

4.1.1 Details of DNS

Direct numerical simulations (DNS) of a channel flow is used as a reference for comparison based on the first four moments of the three velocity components. This has no-slip and no-penetration boundaries at the top and bottom walls and periodic boundary conditions at the lateral walls and in stream-wise direction and it was executed at a shear Reynolds number of $Re_\tau = 350$. It was set up and executed by Hadi Sichani (2021) with a Fourier-Chebyshev pseudo-spectral solver (Zonta et al., 2012). The approximate bulk Reynolds number computed with the channel height $(2h)$ is $Re_b = 12 \times 10^3$ (estimation given by Pope (2001)). The grid is $512 \times 513 \times 512$ collocation points in stream-wise (x), wall-normal (y), and span-wise (z) directions respectively. The domain spans $4\pi h \times 2h \times 2\pi h$ in x, y, and z respectively. The theoretical width-to-height aspect ratio is $AR = \infty$, because of the periodic lateral boundaries. The results are averaged in stream-wise direction, but also in time. The averaging time window is 1500 viscous lengths.

4.2 Eulerian data export

The software `DAVIS` (La Vision G.m.b.H.) integrating the algorithm - Shake-The-Box (Schanz et al., 2016)) - responsible for computing tracer trajectories from the images captured by the cameras is also responsible for transforming this information into a more commonly used arrangement. Usually

S.	Type	Syst.	Re_τ	Sub-vol. voxel	Overlap	Init. spac. l_τ	Fin. grid voxel	Fin. spac. l_τ	Snapshots
–	DNS	channel	350	-	-	-	-	-	-
●	Exp.	duct	367	8^3	75%	3	2^3	0.75	600
▲	Exp.	duct	367	16^3	75%	6	4^3	1.5	600
★	Exp.	duct	367	16^3	75%	6	4^3	1.5	4000
▼	Exp.	duct	367	16^3	75%	6	4^3	1.5	12000
■	Exp.	duct	367	32^3	75%	12	8^3	3	600
◆	Exp.	duct	367	64^3	75%	24	16^3	6	600

TABLE 4.1 – Table showing the symbols (S.) associated to the data used to compute the profiles in Fig. 4.1, 4.2, A.1, A.2, A.3, and A.4. The type of investigation and system configuration (Syst.) are listed. The sub-volume size (Sub.-vol.), overlap, and initial bin size (Init. spac.) are also listed. The viscous length is denoted with l_τ. The final Eulerian grid (Fin. grid) and the final spacing (Fin. spac.) are listed. Lastly the amount of snapshots (each $\approx 3 \times 10^4$ traces) considered for the averaging is given. The channel DNS at $Re_\tau = 350$ (−) is shown for reference (Hadi Sichani (2021)).

numerical and experimental studies consider velocity vectors or other quantities, like concentration or temperature, at fixed positions in space. This is referred to as an Eulerian description of the flow. These scalar or vector fields are then used to compute other derived quantities of interest, such as statistical properties. This type of data export here called Eulerian data export means that the Eulerian field has been computed directly in the software DAVIS with the parameters set there.

Ensuring the independence of results with respect to the chosen parameters for data processing is considered here of significance. Table 4.1 summarises the parameter space investigated. Details about the meaning of the varied parameters are given in Sec. 4.2.1 and Sec. 4.2.2. The shear Reynolds number of the experiments in the TU Wien Turbulent Water Channel reported in the Table 4.1 was found by fitting the average stream-wise profile of the measurements to the reference channel DNS. The same is true for the results shown in Sec. 4.4.

4.2.1   Comparison between grid size

The software used for computing the Eulerian velocity fields from the tracer trajectories computed with the Shake-the-Box method needs among others the setting of two key parameters which define the size of interrogation window, i.e. sub-volume size and the overlap between windows. These two define the final grid upon which the Eulerian velocity vectors are placed. The trajectories inside each sub-volume contribute to the velocity vector at the center of the sub-volume. Their distance to this grid point is used as a weight by a Gaussian weighting function to determine their contribution to the centre-point. The overlap setting governs how much two neighbouring sub-volumes overlap, i.e. if and how much the same trajectory contributes to different sub-volumes. This is achieved by translating the interrogation sub-volume by less than one edge length of the sub-volume. The final gird is thus of a higher resolution.

Four different sub-volume sizes are compared in Fig. 4.1 in terms of the
first four moments of the stream-wise velocity. They are also compared
to the reference span-wise periodic channel DNS. In panel a) the averaged
stream-wise velocity shows almost independent results with respect to the
sub-volume size. Below $5y^+$ the largest sub-volumes, 64^3 and 32^3 voxel
show a slight overestimation of the average. A more significant deviation is
observed for the same sub-volume sizes in the variance in panel b). Both
underestimate the channel profile between 10 and $30y^+$. Closest to the wall,
below $10y^+$ they deviate significantly from the reference channel DNS profile
but also from the smallest two sub-volume sizes, 8^3 and 16^3 voxels. Here it is
worth considering that 32 voxel as the edge length of the interrogation sub-
volume corresponds to $\approx$ 12 viscous lengths. Because velocities of tracers
so far away from the interrogation window center are used and because of
the high velocity gradients so close to the wall, high errors are expected and
observed. An overestimation of the variance for all data sets is observed
also upwards of $60y^+$. In terms of skewness and flatness in panels c) and d)
all data sets exhibit similar behaviour, with some exceptions. The smallest
sub-volume, i.e. 8^3 voxel shows significantly more noise closer to the center-
line than the other in the flatness profile.

The statistics of the wall-normal and span-wise velocity components
for different interrogation sub-volume sizes are compared in Fig. A.1 and
Fig. A.2. The average wall-normal velocity over the wall-normal direction
in panel a) of Fig. A.1 is largely independent on the data set. The pro-
files show the same deviation from the reference channel DNS. In panel b)
it is observable that the data set 8^3 voxel shows higher overestimation of
the variance than the other sub-volume sizes. From the skewness and flat-
ness profiles significant noise is observable for the smallest sub-volume size.
Similar observations can also be made about the first four moments of the
span-wise velocity in Fig. A.2. Nonetheless judging by the flatness profile
in panel d) it is noticeable that the sub-volume size of 16^3 voxel is able to
better follow the channel DNS profile. The other data sets are just noise
and no trend can be observed.

In summary similar behaviours are observed between the four studied
sub-volume sizes in terms of stream-wise velocity statistics. Nonetheless
the size of 16^3 voxel edge length (equivalent to 6 viscous lengths) showed
the best agreement with the reference statistically one-dimensional channel
obtained by DNS.

4.2.2   Comparison between different amount of data

As discussed in Sec. 4.2.1 the measurement data exported with an interro-
gation window of $\approx 1.5y^+$ edge length, i.e. $16 \times 16 \times 16$ voxel with 75%
overlap, shows good agreement with the results obtained by direct numer-
ical simulation in channel flow. For this reason the investigation of how
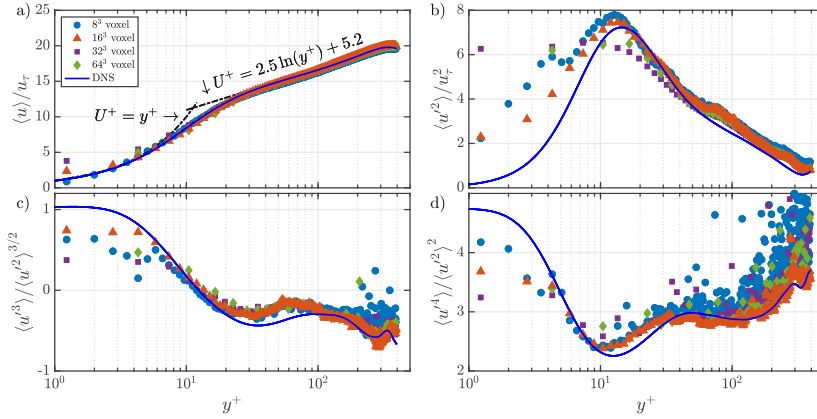these results change with increasing amount of measurement data seems

FIGURE 4.1 – A comparison of the sub-volume binning size based on the first four moments of velocity in stream-wise direction is shown. The binning sizes of 8^3 (blue dot), 16^3 (orange triangle), 32^3 (violet square), and 64^3 (green rhombus) voxels have been chosen and are shown here. An overlap of 75% has been used. The shear Reynolds number $Re_\tau = 367$ and the side length of 8 voxels corresponds to ≈ 3 viscous lengths. The averaging has been done over 600 snapshots, in each $\approx 3 \times 10^4$ tracers tracks have been identified. Profiles of a DNS at $Re_\tau = 350$ in channel flow are also plotted (blue line)(Courtesy of Hadi Sichani (2021)). Panel a) and panel b) show the average stream-wise velocity and average stream-wise Reynolds normal-stress profile respectively over the wall-normal direction scaled by inner variables. Panel c) shows the skewness and panel d) shows the flatness of the stream-wise velocity over the wall-normal direction. The abscissa of panel c) and d) apply to panel a) and d) respectively.

warranted. Measurements have been done over 150 cycles consisting of 81 snapshots spaced by $1\,\mathrm{ms}$ in time. The time between the cycles is of the order of seconds. If the velocity of the largest eddy is of the order of the center-line velocity and the length scale is of the order of the half-height, then the eddy turn-over time is $t_e \approx h/u_c = 0.04\,\mathrm{m}/0.2\,\mathrm{m\,s^{-1}} = 200\,\mathrm{ms}$. Fig. 4.2, Fig. A.3, and Fig. A.4 show the velocity components statistics of three different data sets: 0.6×10^3, 4×10^3, and 12×10^3 snapshots in time. For the first, second, and third data sets 4, 27, and 81 equally spaced snapshots were used for the computation of the first four moments. Thus some snapshots are correlated in time, but due to the large amount of independent cycles measured, an argument can be made that the largest eddy is sampled at different moments during its turnover. In this way the dynamics are represented equivocally in the averaging procedure.

The first four moments of the stream-wise velocity over the wall normal direction are reported in Fig. 4.2. The wall-normal and span-wise results are reported in Fig. A.3 and Fig. A.4, respectively. By observing these three figures with four panels each showing average, variance, skewness, and flatness profiles over the wall-normal direction, it is clear that increasing the amount of considered data had almost no effect on the computed statistics. This shows that 600 snapshots in time for this configuration are sufficient to cap-
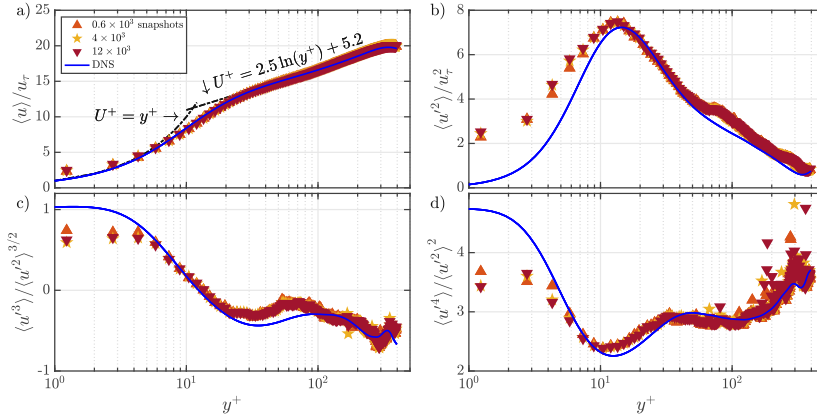
FIGURE 4.2 – A comparison of the amount of data based on the first four moments of velocity in stream-wise direction is shown. The binning size of 16^3 voxels has been chosen and an overlap of 75% has been used. The shear Reynolds number is $Re_\tau = 367$. The averaging has been done over 0.6×10^3 (orange triangle), 4×10^3 (yellow pentagram), and 12×10^3 (red downward triangle) snapshots respectively. In each $\approx 3 \times 10^4$ tracers tracks have been identified. Profiles of a DNS at $Re_\tau = 350$ in channel flow are also plotted (blue line)(Courtesy of Hadi Sichani (2021)). Panel a) and panel b) show the average stream-wise velocity and average stream-wise Reynolds normal-stress profile respectively over the wall-normal direction scaled by inner variables. Panel c) shows the skewness and panel d) shows the flatness of the stream-wise velocity over the wall-normal direction. The abscissa of panel c) and d) apply to panel a) and d) respectively.

ture the essential behaviour of the quantities of interest. Nonetheless using more data for computing the statistics improves the confidence intervals (not shown in this work) for a give confidence level (Pope, 2001). The reporting of these intervals is mandatory when publishing measurement results and many published works on the topic of turbulent wall-bounded flows include confidence intervals or at least a discussion about the expected uncertainty. Here a couple examples are given: Kasagi and Matsunaga (1995), Hoyas and Jiménez (2006), Gurka et al. (2006), Marusic et al. (2013), Wilson and Smith (2013), Schultz and Flack (2013), and Vinuesa et al. (2014). Due to restricted resources, the publication of confidence intervals are reserved for the future.

4.3   Lagrangian data export

With the aim of providing evidence independent of the data processing technique, a second data export type is carried out and investigated. The first type, called Eulerian data export was discussed in Sec. 4.2. The Lagrangian data export, which this section is dedicated to, means that the trajectories computed by the algorithm Shake-The-Box have been exported directly.

These were then used by myself to generate the Eulerian velocity fields in a more straight-forward way and significantly less computationally expensive. An equidistant grid fixed in space was first generated with a certain grid spacing. The positions of all the tracers were identified. For each grid point one tracer was searched in its vicinity. The searched volume is a cube with side length of one grid spacing and is centred around the grid point. The velocity of the tracer found within this searched volume was used directly as the velocity at the grid point. The results of this type of data export is also an Eulerian velocity field. The programs responsible for generating the Eulerian velocity field and statistics computation have been written by myself, so the procedure and algorithm is fully understood and documented, unlike the procedure described in Sec. 4.2.

4.3.1   Comparison between grid size

The only parameter which can be chosen for the Lagrangian data export procedure is the grid spacing. This defines the precision of the tracer velocity assignment to the grid points. A comparison between two grid spacings: 1 and 5 viscous lengths (l_τ) are compared in terms of the first four moments of the stream-wise velocity in Fig. 4.3. The results of the measurements are compared with the reference channel obtained by DNS (details are given in Sec. 4.1.1). For the average stream-wise velocity in panel a) of Fig. 4.3 it is observed that the choice of grid spacing had no effect on the profile as both investigated grids overlapped with the reference, except that the resolution of the profile is reduced. In panel b) of the same figure the variance computed on the smallest investigated grid spacing follows the reference profile closer that the largest one. The grid of $5l_\tau$ overestimates the variance below $10y^+$. It also underestimates the skewness and flatness in panel c) and d), respectively below $5y^+$. This is to be expected as this is the edge length of the interrogation volume. For the rest of the height of the duct both grids reproduce the span-wise periodic statistically one-dimensional channel results (DNS) in terms of average, variance, skewness, and flatness. The other two components, wall-normal and span-wise are shown in Fig. A.5 and Fig. A.6, respectively. Here both grids are able to reproduce the same behaviour. There is little difference between them, but they do deviate from the reference DNS. These differences are more closely discussed in Sec. 4.4, where both data export procedures are compared to the channel DNS.

4.4   Comparison lagrangian, eulerian and DNS

In order to ensure that the choice of technique which generates the Eulerian velocity field has no impact on the results, the results of the two discussed techniques are compared with the channel DNS in Fig. 4.4. The first obser-
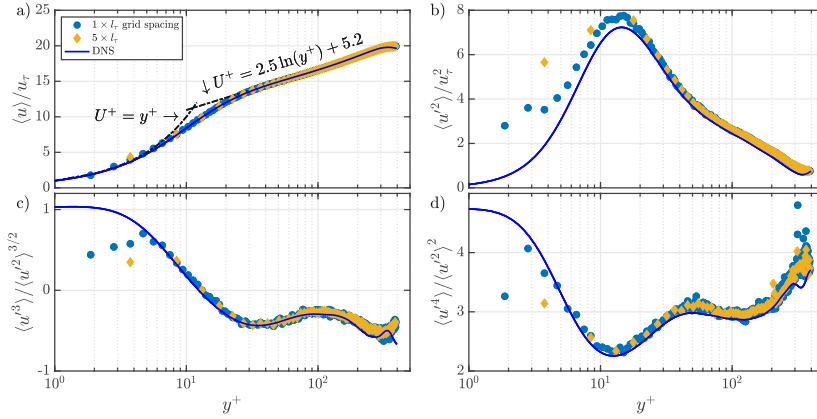
FIGURE 4.3 – A comparison of the grid size based on the first four moments of velocity in stream-wise direction is shown. The shear Reynolds number is $Re_\tau = 375$. The averaging has been done over 0.8×10^3 independent snapshots (each $\approx 3 \times 10^4$ tracers). The grid spacings are 1 (blue dot) and 5 (yellow rhombus) viscous lengths. Profiles of a DNS at $Re_\tau = 350$ in channel flow are also plotted (blue line)(Courtesy of Hadi Sichani (2021)). Panel a) and panel b) show the average stream-wise velocity and average stream-wise Reynolds normal-stress profile respectively over the wall-normal direction scaled by inner variables. Panel c) shows the skewness and panel d) shows the flatness of the stream-wise velocity over the wall-normal direction. The abscissa of panel c) and d) apply to panel a) and d) respectively.

vation is that the results are mostly independent on the type of data export. This is significant because the Eulerian data export involves a computationally expensive step in which the assigned velocities to the grid points are a weighted average of the velocities of the tracers in the vicinity. The weights are decided by a Gaussian weighting function based on the distance of the tracer to the grid point (see Sec. 4.2.1). The second central observation is that for the stream-wise velocity, the measured statistics are in good agreement with the ones obtained from direct numerical simulations in channel flow. In panel a) Fig. 4.4 the average stream-wise profiles overlap over the whole duct half-height with the results of DNS, but also with the law-of-the-wall: in the log-layer a Kármán constant of $\kappa = 0.4$ and an increment of 5.2 are shown. The variance, or main Reynolds stresses in panel b) of the same figure are being overestimated close to the wall under $y^+ = 20$ for both processing techniques. A similar observation can be made about the skewness - panel c) - and flatness - panel d) - in the viscous sub-layer: they are both underestimated. One reason for the higher errors so close to the wall ($y^+ = 5$ is equivalent to $540\,\mu m$ above the wall) could be the difficulty of tracking particles in such close proximity to the wall due to optical interference with the surface. The Lagrangian data export (explained in Sec. 4.3.1) shows higher noise close to the center line in the flatness. Overall the first four moments of the stream-wise velocity measured by means of 3D

PTV in the TU Wien Turbulent Water Channel show good agreement with the results obtained by direct numerical simulation in a span-wise periodic channel - a statistically one-dimensional and stationary turbulent flow.
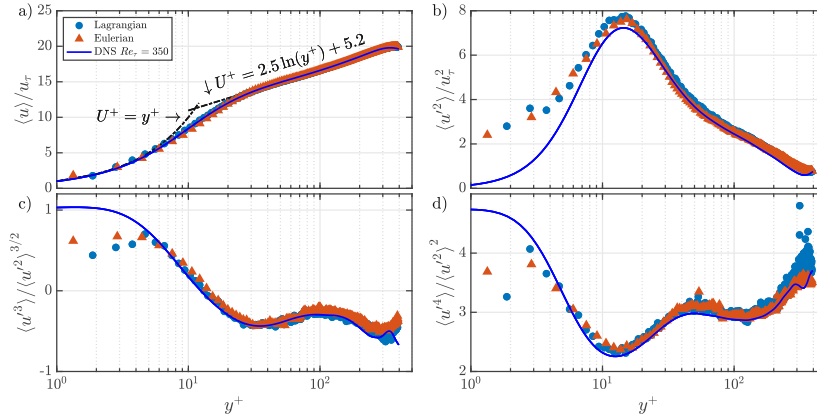

FIGURE 4.4 – A comparison of the post-processing technique based on the first four moments of velocity in stream-wise direction is shown. The shear Reynolds number is $Re_\tau = 375$. The averaging havs been done over 0.8×10^3 snapshots (each $\approx 3 \times 10^4$ tracers). The Lagrangian data export has a grid spacing of 1 viscous length (orange square). The Eulerian data has a binning size of 16^3 voxels (≈ 6 viscous lengths) and an overlap of 75% (orange triangles). Profiles of a DNS at $Re_\tau = 350$ in channel flow are also plotted (blue line)(Courtesy of Hadi Sichani (2021)). Panel a) and panel b) show the average stream-wise velocity and average stream-wise Reynolds normal-stress profile respectively over the wall-normal direction scaled by inner variables. Panel c) shows the skewness and panel d) shows the flatness of the stream-wise velocity over the wall-normal direction. The abscissa of panel c) and d) apply to panel a) and d) respectively.

The results of both processing techniques are also compared with the profiles of the DNS based on the first four moments of the two other velocity components, wall-normal (v), and span-wise (w) in Fig. A.7 and Fig. A.8 respectively. The average wall-normal velocity shows a deviation of less that $0.15u_\tau$ from zero. The wall-normal averaged velocity in the channel is zero over the whole half-height, because there is no average forcing driving the flow in the wall-normal direction. This deviation could be indicative of misalignment of the measurements coordinate system (defined by the calibration target placed by hand in the duct) with the laboratory coordinate system, i.e. main flow direction. A similar argument can be made about the average span-wise velocity component (panel a) of Fig. A.8). Sec. 4.5 discusses a proposed method for improving these results. The profiles of Reynolds stresses $\langle v'v' \rangle$ (panel b) of Fig. A.7) show satisfactory agreement with the channel DNS. Closer to the wall (under $y^+ = 30$) they are overestimated by both the Lagrangian and Eulerian data exports. The skewness profiles show good agreement with the reference, except higher noise exhibited by the Lagrangian data export below $y^+ = 10$. In panel d) the

flatness profiles show a near overlap with the channel results, except for the Eulerian data export which underestimates the likelihood of extreme events in the region under 20 viscous lengths away from the wall. The Reynolds stresses $\langle w'w' \rangle$ profiles (panel b) of Fig. A.8) show an overestimation across the whole half-height by both data processing techniques. The overlap of the Eulerian data export with the peak shown by the DNS seems coincidental. The skewness profiles show good agreement with the reference, except for the higher noise present in the results of the Lagrangian data export throughout the whole duct half-height. The flatness is overestimated by the Lagrangian data export, while the Eulerian one shows good agreement with the reference above $y^+ = 20$.

In summary the first four moments of the measured velocity field in the TU Wien Turbulent Water Channel (stream-wise u, wall-normal v, and span-wise w in Fig. 4.4, Fig. A.7, and Fig. A.8 respectively) show good agreement with the statistically one-dimensional stationary turbulent channel flow achieved by direct numerical simulations. The statistics of the wall-normal and span-wise components could be improved by techniques described in Sec. 4.5 or by a more accurate placement of the calibration target in the experimental facility.

4.5   Misalignment correction

The accuracy of measurement of tracer positions over time and thus their velocities, as precursors of Eulerian velocity fields, is affected by the alignment of the measurement volume with the laser illuminated volume. Rama Reddy et al. (2016) investigated the effects of this misalignment on the root-mean-square of the velocities for Stereoscopic-PIV measurements. They used direct numerical simulations and experiments at shear-Reynolds number of $Re_\tau \approx 934$. They concluded that $1°$ of angular misalignment and a translational misalignment of a half-thickness of laser sheet has a negligible effect on the mentioned statistics. Another possible source of inaccuracy in our velocimetry procedure is the misalignment of the calibration plate with the main flow direction. The position of this plate is of importance, because it defines the position and tilt of the coordinate system used for the measurements with respect to the main direction of the flow and walls of the duct. The calibration plate used for the cameras is placed inside the water channel without a mechanically repeatable procedure for defining or measuring its position or inclination angles with respect to the walls, save for an optical check, consisting of a tape strip which guides the experimenter to an approximate position of the laser illuminated volume. A misalignment will result in erroneous measurement of the velocity components as they will not correspond with the actual stream-wise, span-wise, and wall-normal components. In order to correct for this misalignment as a first approximation the following procedure is proposed: if the angles α and θ are the inclination

angles of the calibration plate with respect to the stream-wise (Fig. 4.5) and wall-normal (Fig. 4.6) directions respectively and the measured velocity components are $\tilde{u}$, $\tilde{v}$, and $\tilde{w}$ then the actual stream-wise, span-wise, and wall-normal components are u, v, and w:

$$u(x, y, z, t) = \tilde{u} \cos \alpha + \tilde{w} \cos \theta \sin \alpha + \tilde{v} \sin \theta \sin \alpha \ , \tag{4.1}$$

$$v(x, y, z, t) = -\tilde{w} \sin \theta + \tilde{v} \cos \theta \ , \tag{4.2}$$

$$w(x, y, z, t) = -\tilde{u} \sin \alpha + \tilde{w} \cos \theta \cos \alpha + \tilde{v} \sin \theta \cos \alpha \ . \tag{4.3}$$

As the angles α and θ have not been measured and are unknown the following assumptions have to be made to compute them:

- due to non-existent average forcing in span-wise direction: the averaged span-wise velocity component is zero: $\langle w(y) \rangle_t = 0$,

- due to non-existent average forcing in wall-normal direction: the averaged wall-normal velocity component is zero: $\langle v(y) \rangle_t = 0$,

- the inclination angles α and θ of the calibration plate are constant for all times and all locations in space on the calibration plate.
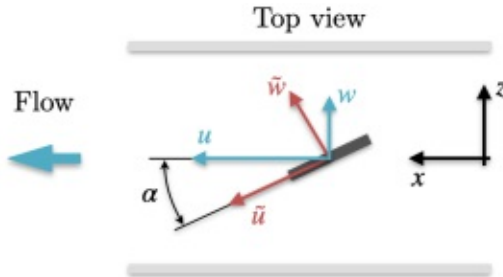

FIGURE 4.5 – A simplified schematic of the calibration target placed in the TU Wien Turbulent Water Channel from the top view is shown. The misalignment angle α of the measurement coordinate system defined by the manual placement of the target with respect to the main flow direction is indicated. The velocities $\tilde{u}$ and $\tilde{w}$ are obtained by measurement. The quantities u and w are the ones searched for. The schematic is not to scale.

Averaging over time equations 4.1 - 4.3 and using the previously mentioned assumptions, one can find a first estimate for the misalignment angles averaged over the measurement volume:

$$\alpha = \left\langle \arctan \left(\frac{\langle \tilde{w} \rangle_t \cos \theta + \langle \tilde{v} \rangle_t \sin \theta}{\langle \tilde{u} \rangle_t} \right) \right\rangle_{x,y,z} \ , \tag{4.4}$$

$$\theta = \left\langle \arctan \left(\frac{\langle \tilde{v} \rangle_t}{\langle \tilde{w} \rangle_t} \right) \right\rangle_{x,y,z} \ . \tag{4.5}$$
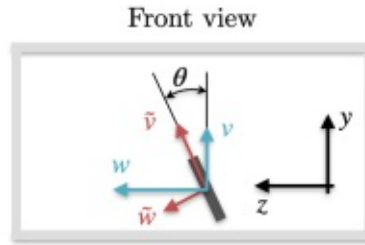
Front view

FIGURE 4.6 – A simplified schematic of the calibration target placed in the TU Wien Turbulent Water Channel from the front view is shown. The misalignment angle θ of the measurement coordinate system defined by the manual placement of the target with respect to the wall-normal direction is indicated. The velocities $\tilde{v}$ and $\tilde{w}$ are obtained by measurement. The quantities v and w are the ones searched for. The schematic is not to scale.

These angles are used to correct the measured fields $\tilde{u}$, $\tilde{v}$, and $\tilde{w}$. Thus the desired corrected fields u, v, and w are computed from Eq. (4.1) - (4.3). The results are compared in Fig. 4.7 in terms of the span-wise velocity components based on the first four moments. It is observable that for the uncorrected results, the measured average span-wise velocity is non-zero. This is not physical because there is no average forcing in the span-wise direction in the TU Wien Water Turbulent Channel. Moreover the error increases closer to the centre line. This could be due to the stream-wise velocity measured in the misaligned coordinate system influencing the span-wise velocity in the laboratory coordinate system by virtue of Eq. (4.3). The proposed correction improves this error, evident in panel a) of Fig. 4.7, but does not manage to improve the other three statistics, variance, skewness, and flatness shown in panel b), c), and d) respectively. The significance of this correction cannot be appreciated by comparison with the average span-wise profile, which is ideally zero (if the averaging in the DNS is done over much longer times than the ones considered here). At the center line the order of error in the average is $\approx 0.3u_\tau$. Comparing this with the magnitude of span-wise fluctuations in terms of $\langle w'^2 \rangle^{1/2} \approx 0.67u_\tau$ (for the DNS profile) it is reasonable to think that the correction is meaningful, i.e. it can significantly improve the performed measurements. This could indicate that a more controlled placement of the calibration target is needed to improve the span-wise and wall-normal velocity profiles. The stream-wise and wall-normal components are reported in Appendix A in Fig. A.10 and Fig. A.9 respectively. They show no appreciable difference between the two data sets, corrected and uncorrected. In terms of the stream-wise component this is to be expected. The average wall-normal velocity component is not corrected contrary to expectations. It is possible that the misalignment correction works on this component as well if an iterative procedure is defined, where the corrected velocity fields are used for approximating new misalignment angles. They

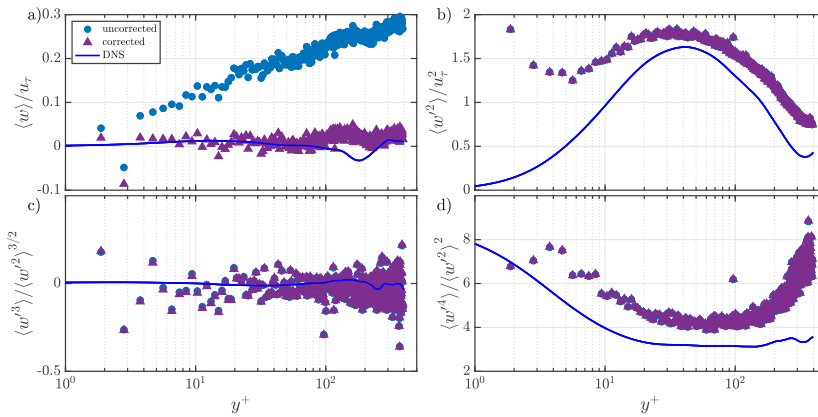could be then used to correct a second time the first correction.

FIGURE 4.7 – The effect of misalignment correction on the first four moments of the span-wise velocity is shown. The shear Reynolds number is $Re_\tau = 375$. The averaging has been done over 0.8×10^3 snapshots (each $\approx 3 \times 10^4$ tracers) and the grid spacing is ≈ 1 viscous length. The iterative procedure for correction is described in Sec. 4.5 .The uncorrected (blue dot) and corrected (violet triangle) results are shown. Profiles of a DNS at $Re_\tau = 350$ in channel flow are also plotted (blue line)(Courtesy of Hadi Sichani (2021)). Panel a) and panel b) show the average span-wise velocity and average span-wise Reynolds normal-stress profile respectively over the wall-normal direction scaled by inner variables. Panel c) shows the skewness and panel d) shows the flatness of the span-wise velocity over the wall-normal direction. The abscissa of panel c) and d) apply to panel a) and d) respectively.

5

Conclusions

The aim of this work is to provide evidence that the duct flow in the TU Wien Turbulent Water Channel is statistically one-dimensional, i.e. that the lateral walls have no influence on the flow in the center plane (span-wise) of the facility and the average quantities do not vary in the stream-wise direction. This ensures that future studies will be carried out in ideal conditions. The experimental duct has a width-to-height aspect ratio of 10. The flow was investigated at a shear Reynolds number of ≈ 370. The measurements were obtained by a high speed three dimensional three component particle tracking velocimetry setup. The first four statistical moments of the stream-wise velocity component showed a good agreement between the measurements and the results of a channel flow which was statistically one-dimensional and stationary. The reference results were obtained by direct numerical simulation. Moreover different techniques for exporting and processing the velocimetry data and different parameters, such as grid spacing and amount of data, have been tried and compared in order to ensure that these results were not coincidental. The other two velocity components showed reasonable agreement with the reference and a correction of these profiles has been proposed. The correction was able to improve the average span-wise velocity, while it remained unable to improve the other quantities of interest. This indicated that an accurate placement of the calibration target in the experimental facility may be of significance if the experiment aims to correctly capture span-wise and wall-normal motion of anisotropic particles, such as deformable fibres in a turbulent flow field. The technique and mechanism for the accurate placement of the target remain reserved for the future. An additional correction of the misalignment of the laser sheet with the measurement volume (Rama Reddy et al., 2016) is reserved for the future. Moreover some aspects regarding facility control are to be improved in the close future: real-time volumetric flow rate and temperature measurement and an automatic control of the pump. This will allow the experimenter to set a desired bulk Reynolds number. This flow will then be achieved by the automatic systems of the facility.

The whole range of possible Reynolds numbers in the TU Wien Tur-

bulent Water Channel will be explored. New measurements at different span-wise and stream-wise locations are planned in order to provide final evidence of the statistical homogeneity in these directions.

It was found through direct numerical simulations that a duct of width-to-height aspect ratio of 8 is not sufficient at a shear Reynolds number of 150 to approximate a statistically one-dimensional stationary channel flow produced by DNS. For the future the simulation of higher aspect ratio ducts at higher Reynolds numbers is reserved. These results will be compared directly with the measurements in the experimental facility. Moreover the accurate control of the shear Reynolds number among all compared simulations will be aimed for.

Lastly a new configuration of the experimental facility will be set up in order to measure interactions between anisotropic particles with the turbulent flow field over a large span-wise and stream-wise region in the immediate vicinity of the ducts bottom wall.

A

Appendix

This appendix serves the purpose of publishing and archiving important results which are too extensive to be shown in the main document. Without these results the quantitative assessment of the single phase turbulent flow field in the TU Wien Turbulent Water Channel is incomplete.

A.1   Eulerian data export

A.1.1   Comparison between grid size

In this section the effect of different grid spacing of the Eulerian data export are compared in terms of the first four moments of the wall-normal (Fig. A.1) and span-wise (Fig. A.2) velocity components. They are also compared to the reference direct numerical simulation of a span-wise periodic channel. The reader is referred to Sec. 4.2.1 for the discussion of these figures.
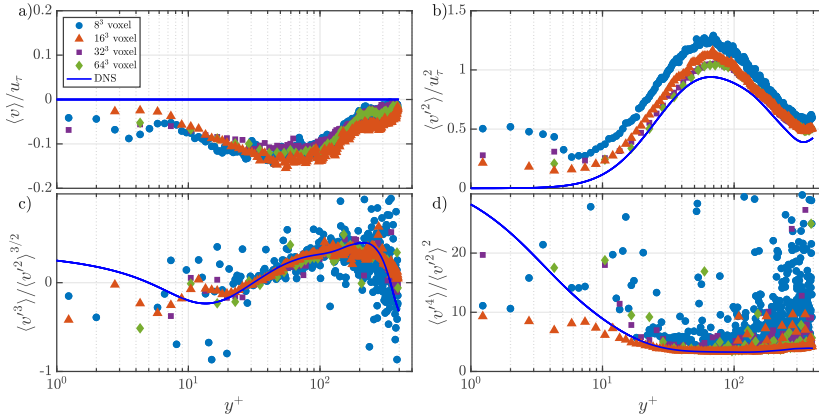

FIGURE A.1 – A comparison of the sub-volume binning size based on the first four moments of velocity in wall-normal direction is shown. The binning sizes of 8^3 (blue dot), 16^3 (orange triangle), 32^3 (violet square), and 64^3 (green rhombus) voxels have been chosen and are shown here. An overlap of 75% has been used. The shear Reynolds number $Re_\tau = 367$ and the side length of 8 voxels corresponds to ≈ 3 viscous lengths. The averaging has been done over 600 snapshots, in each $\approx 3 \times 10^4$ tracers tracks have been identified. Profiles of a DNS at $Re_\tau = 350$ in channel flow are also plotted (blue line)(Courtesy of Hadi Sichani (2021)). Panel a) and panel b) show the average wall-normal velocity and average wall-normal Reynolds normal-stress profile respectively over the wall-normal direction scaled by inner variables. Panel c) shows the skewness and panel d) shows the flatness of the wall-normal velocity over the wall-normal direction. The abscissa of panel c) and d) apply to panel a) and d) respectively.
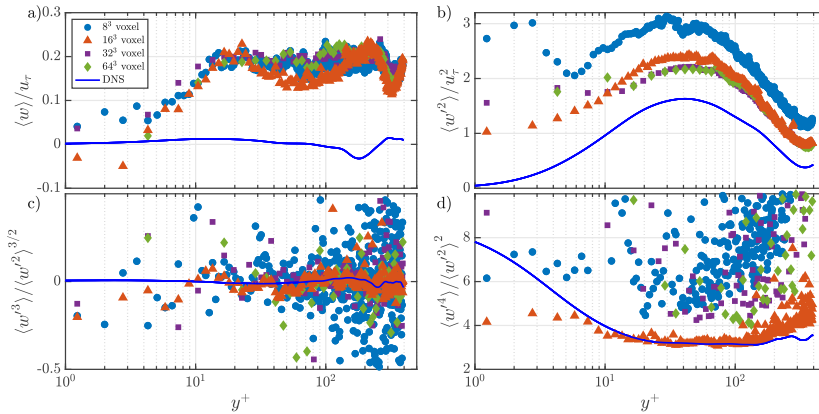
FIGURE A.2 – A comparison of the sub-volume binning size based on the first four moments of velocity in span-wise direction is shown. The binning sizes of 8^3 (blue dot), 16^3 (orange triangle), 32^3 (violet square), and 64^3 (green rhombus) voxels have been chosen and are shown here. An overlap of 75% has been used. The shear Reynolds number $Re_\tau = 367$ and the side length of 8 voxels corresponds to ≈ 3 viscous lengths. The averaging has been done over 600 snapshots, in each $\approx 3 \times 10^4$ tracers tracks have been identified. Profiles of a DNS at $Re_\tau = 350$ in channel flow are also plotted (blue line)(Courtesy of Hadi Sichani (2021)). Panel a) and panel b) show the average span-wise velocity and average span-wise Reynolds normal-stress profile respectively over the wall-normal direction scaled by inner variables. Panel c) shows the skewness and panel d) shows the flatness of the span-wise velocity over the wall-normal direction. The abscissa of panel c) and d) apply to panel a) and d) respectively.

A.1.2 Comparison between different amount of data

In this section different amount of snapshots in time of the Eulerian data export are compared in terms of the first four moments of the wall-normal (Fig. A.3) and span-wise (Fig. A.4) velocity components. They are also compared to the reference direct numerical simulation of a span-wise periodic channel. The reader is referred to Sec. 4.2.2 for the discussion of these figures.
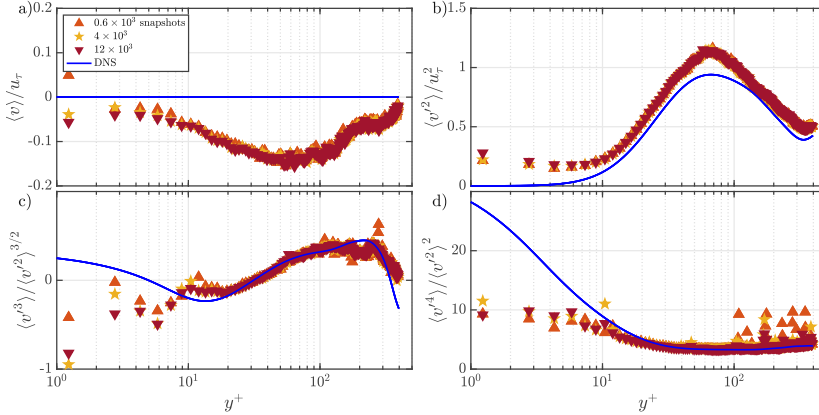

FIGURE A.3 – A comparison of the amount of data based on the first four moments of velocity in wall-normal direction is shown. The binning size of 16^3 voxels has been chosen and an overlap of 75% has been used. The shear Reynolds number is $Re_\tau = 367$. The averaging has been done over 0.6×10^3 (orange triangle), 4×10^3 (yellow pentagram), and 12×10^3 (red downward triangle) snapshots respectively. In each $\approx 3 \times 10^4$ tracers tracks have been identified. Profiles of a DNS at $Re_\tau = 350$ in channel flow are also plotted (blue line)(Courtesy of Hadi Sichani (2021)). Panel a) and panel b) show the average wall-normal velocity and average wall-normal Reynolds normal-stress profile respectively over the wall-normal direction scaled by inner variables. Panel c) shows the skewness and panel d) shows the flatness of the wall-normal velocity over the wall-normal direction. The abscissa of panel c) and d) apply to panel a) and d) respectively.
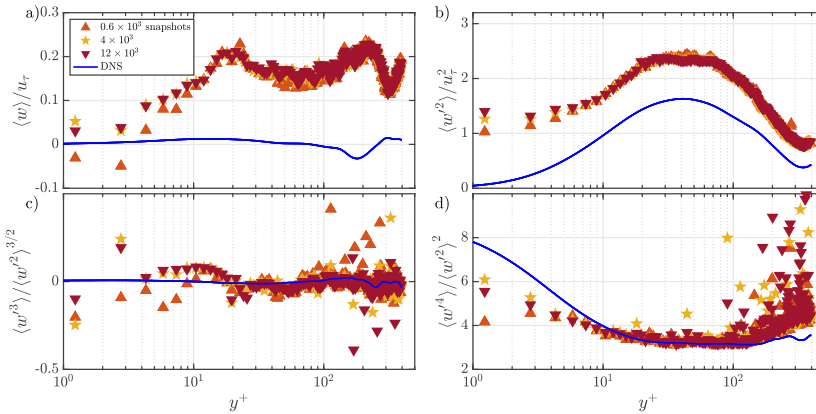
FIGURE A.4 – A comparison of the amount of data based on the first four moments of velocity in span-wise direction is shown. The binning size of 16^3 voxels has been chosen and an overlap of 75% has been used. The shear Reynolds number is $Re_\tau = 367$. The averaging has been done over 0.6×10^3 (orange triangle), 4×10^3 (yellow pentagram), and 12×10^3 (red downward triangle) snapshots respectively. In each $\approx 3 \times 10^4$ tracers tracks have been identified. Profiles of a DNS at $Re_\tau = 350$ in channel flow are also plotted (blue line)(Courtesy of Hadi Sichani (2021)). Panel a) and panel b) show the average span-wise velocity and average span-wise Reynolds normal-stress profile respectively over the wall-normal direction scaled by inner variables. Panel c) shows the skewness and panel d) shows the flatness of the span-wise velocity over the wall-normal direction. The abscissa of panel c) and d) apply to panel a) and d) respectively.

A.2   Lagrangian data export

A.2.1   Comparison between grid size

In this section both grid sizes of the Lagrangian data export have compared in terms of the first four moments of the wall-normal (Fig. A.5) and span-wise (Fig. A.6) velocity components. They are also compared to the reference direct numerical simulation of a span-wise periodic channel. The reader is referred to Sec. 4.3.1 for the discussion of these figures.
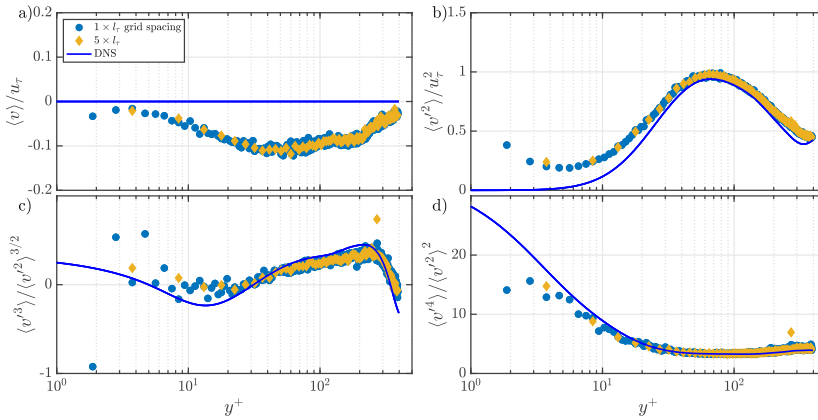

FIGURE A.5 – A comparison of the grid size based on the first four moments of velocity in wall-normal direction is shown. The shear Reynolds number is $Re_\tau = 375$. The averaging has been done over 0.8×10^3 independent snapshots (each $\approx 3 \times 10^4$ tracers). The grid spacings are 1 (blue dot) and 5 (yellow rhombus) viscous lengths. Profiles of a DNS at $Re_\tau = 350$ in channel flow are also plotted (blue line)(Courtesy of Hadi Sichani (2021)). Panel a) and panel b) show the average wall-normal velocity and average wall-normal Reynolds normal-stress profile respectively over the wall-normal direction scaled by inner variables. Panel c) shows the skewness and panel d) shows the flatness of the wall-normal velocity over the wall-normal direction. The abscissa of panel c) and d) apply to panel a) and d) respectively.
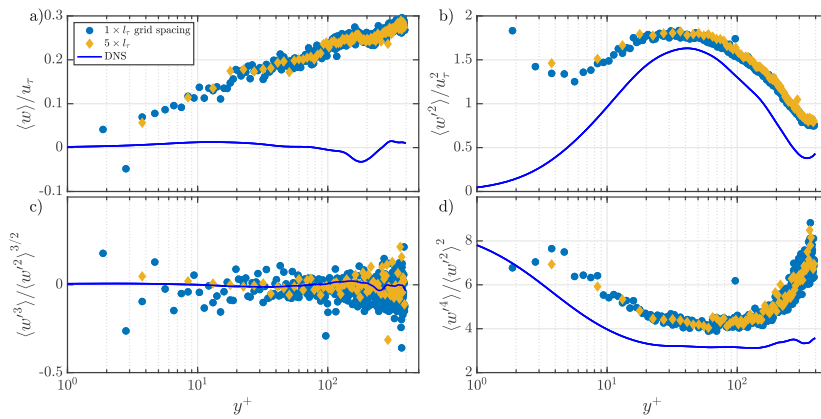
FIGURE A.6 – A comparison of the grid size based on the first four moments of velocity in span-wise direction is shown. The shear Reynolds number is $Re_\tau = 375$. The averaging has been done over 0.8×10^3 independent snapshots (each $\approx 3 \times 10^4$ tracers). The grid spacings are 1 (blue dot) and 5 (yellow rhombus) viscous lengths. Profiles of a DNS at $Re_\tau = 350$ in channel flow are also plotted (blue line)(Courtesy of Hadi Sichani (2021)). Panel a) and panel b) show the average span-wise velocity and average span-wise Reynolds normal-stress profile respectively over the wall-normal direction scaled by inner variables. Panel c) shows the skewness and panel d) shows the flatness of the span-wise velocity over the wall-normal direction. The abscissa of panel c) and d) apply to panel a) and d) respectively.

A.3   Comparison lagrangian, eulerian and DNS

In this section both types of data exports, Eulerian and Lagrangian are compared to the reference direct numerical simulation of a span-wise periodic channel in terms of the first four moments of the wall normal (Fig. A.7) and span-wise (Fig. A.8) velocity components. Details about the processing of the measurement data are given in Sec. 4.3 and Sec. 4.2. The reader is referred to Sec. 4.4 for the discussion of these figures.
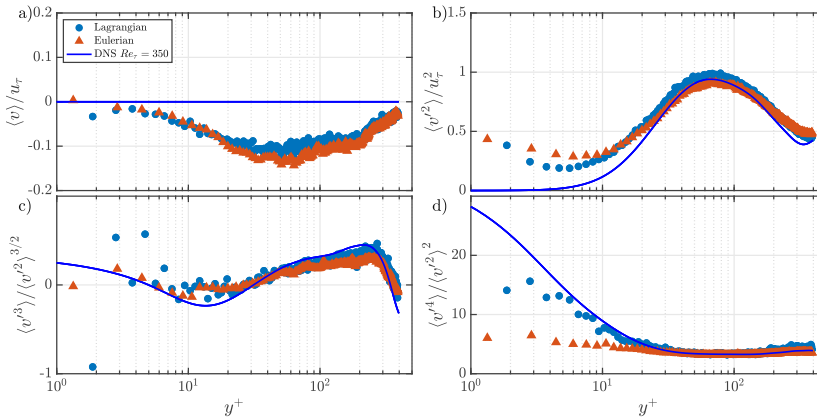

FIGURE A.7 – A comparison of the post-processing technique based on the first four moments of velocity in wall-normal direction is shown. The shear Reynolds number is $Re_\tau = 375$. The averaging has been done over 0.8×10^3 snapshots (each $\approx 3 \times 10^4$ tracers). The Lagrangian data export has a grid spacing of 1 viscous length (orange square). The Eulerian data has a binning size of 16^3 voxels (≈ 6 viscous lengths) and an overlap of 75% (orange triangles). Profiles of a DNS at $Re_\tau = 350$ in channel flow are also plotted (blue line)(Courtesy of Hadi Sichani (2021)). Panel a) and panel b) show the average wall-normal velocity and average wall-normal Reynolds normal-stress profile respectively over the wall-normal direction scaled by inner variables. Panel c) shows the skewness and panel d) shows the flatness of the wall-normal velocity over the wall-normal direction. The abscissa of panel c) and d) apply to panel a) and d) respectively.
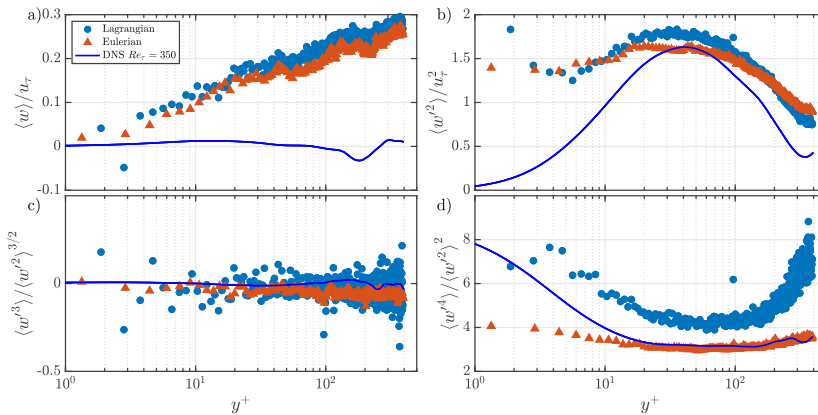
FIGURE A.8 – A comparison of the post-processing technique based on the first four moments of velocity in span-wise direction is shown. The shear Reynolds number is $Re_\tau = 375$. The averaging has been done over 0.8×10^3 snapshots (each $\approx 3 \times 10^4$ tracers). The Lagrangian data export has a grid spacing of 1 viscous length (orange square). The Eulerian data has a binning size of 16^3 voxels (≈ 6 viscous lengths) and an overlap of 75% (orange triangles). Profiles of a DNS at $Re_\tau = 350$ in channel flow are also plotted (blue line)(Courtesy of Hadi Sichani (2021)). Panel a) and panel b) show the average span-wise velocity and average span-wise Reynolds normal-stress profile respectively over the wall-normal direction scaled by inner variables. Panel c) shows the skewness and panel d) shows the flatness of the span-wise velocity over the wall-normal direction. The abscissa of panel c) and d) apply to panel a) and d) respectively.

A.4 Misalignment correction

In this section the effect of the proposed misalignment correction in terms of the first four moments of the wall-normal (Fig. A.9) and stream-wise (Fig. A.10) velocity components. They are also compared to the span-wise periodic channel obtained by direct numerical simulation. Details about the correction procedure are give in Sec. 4.5. The reader is referred to Sec. 4.5 for the discussion of these figures.
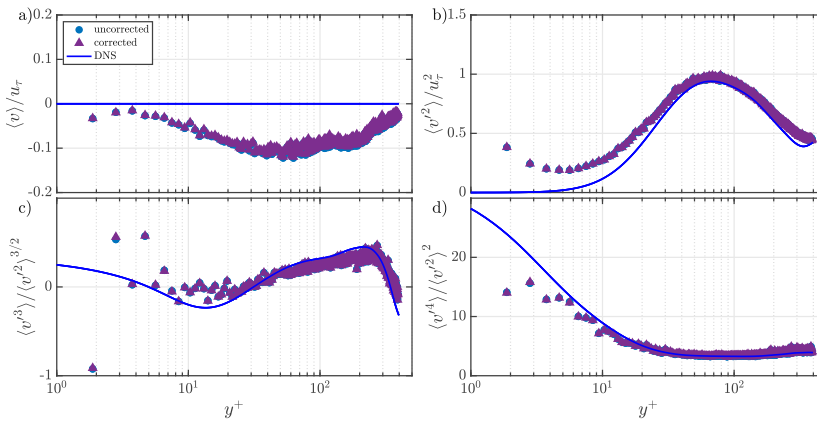

FIGURE A.9 – The effect of misalignment correction on the first four moments of the wall-normal velocity is shown. The shear Reynolds number is $Re_\tau = 375$. The averaging has been done over 0.8×10^3 snapshots (each $\approx 3 \times 10^4$ tracers) and the grid spacing is ≈ 1 viscous length. The iterative procedure for correction is described in Sec. 4.5 .The uncorrected (blue dot) and corrected results are shown. Profiles of a DNS at $Re_\tau = 350$ in channel flow are also plotted (blue line)(Courtesy of Hadi Sichani (2021)). Panel a) and panel b) show the average wall-normal velocity and average wall-normal Reynolds normal-stress profile respectively over the wall-normal direction scaled by inner variables. Panel c) shows the skewness and panel d) shows the flatness of the wall-normal velocity over the wall-normal direction. The abscissa of panel c) and d) apply to panel a) and d) respectively.
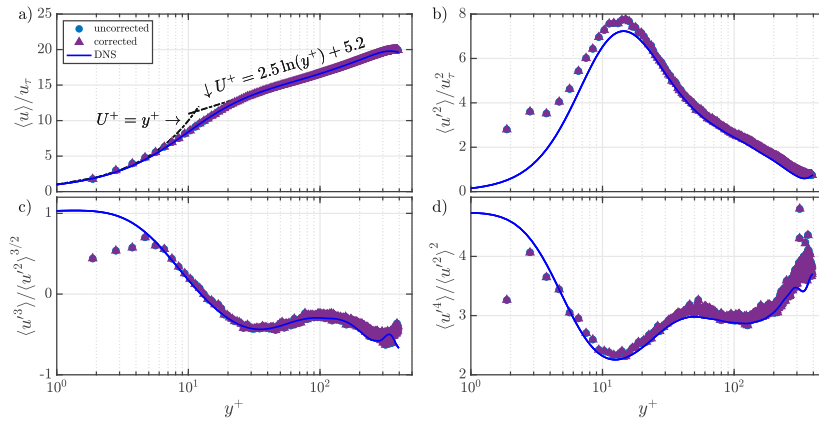
FIGURE A.10 – The effect of misalignment correction on the first four moments of the stream-wise velocity is shown. The shear Reynolds number is $Re_\tau = 375$. The averaging has been done over 0.8×10^3 snapshots (each $\approx 3 \times 10^4$ tracers) and the grid spacing is ≈ 1 viscous length. The iterative procedure for correction is described in Sec. 4.5 .The uncorrected (blue dot) and corrected (violet triangle) results are shown. Profiles of a DNS at $Re_\tau = 350$ in channel flow are also plotted (blue line)(Courtesy of Hadi Sichani (2021)). Panel a) and panel b) show the average stream-wise velocity and average stream-wise Reynolds normal-stress profile respectively over the wall-normal direction scaled by inner variables. Panel c) shows the skewness and panel d) shows the flatness of the stream-wise velocity over the wall-normal direction. The abscissa of panel c) and d) apply to panel a) and d) respectively.

Bibliography

Alipour, M., De Paoli, M., Ghaemi, S., and Soldati, A. (2021). Long non-axisymmetric fibres in turbulent channel flow. *Journal of Fluid Mechanics*, 916:A3.

Antonia, R., Teitel, M., Kim, J., and Browne, L. (1992). Low-Reynolds-number effects in a fully developed turbulent channel flow. *Journal of Fluid mechanics*, 236:579–605.

Cai, W.-H., Li, F.-C., Zhang, H.-N., Li, X.-B., Yu, B., Wei, J.-J., Kawaguchi, Y., and Hishida, K. (2009). Study on the characteristics of turbulent drag-reducing channel flow by particle image velocimetry combining with proper orthogonal decomposition analysis. *Physics of Fluids*, 21(11):115103.

Clark, J. A. (1968). A Study of Incompressible Turbulent Boundary Layers in Channel Flow. *Journal of Basic Engineering*, 90(4):455–467.

Comte-Bellot, G. (1963). Contribution à l'étude de la turbulence de conduite. *These Presente a la Faculte des Sciences de l'Universite de Grenoble*.

Costa, P. (2018). A fft-based finite-difference solver for massively-parallel direct numerical simulations of turbulent flows. *Computers & Mathematics with Applications*, 76(8):1853–1862.

Darcy, H. (1857). *Recherches expérimentales relatives au mouvement de l'eau dans les tuyaux*, volume 1. Mallet-Bachelier.

De Paoli, M. (2021). Direct numerical simulations of turbulent duct and channel flows at $Re_\tau = 150$. *Unpublished*.

Dean, R. and Bradshaw, P. (1976). Measurements of interacting turbulent shear layers in a duct. *Journal of Fluid Mechanics*, 78(4):641–676.

Dean, R. B. (1978). Reynolds Number Dependence of Skin Friction and Other Bulk Flow Variables in Two-Dimensional Rectangular Duct Flow. *Journal of Fluids Engineering*, 100(2):215–223.

Gurka, R., Liberzon, A., and Hetsroni, G. (2006). POD of vorticity fields: A method for spatial characterization of coherent structures. *International Journal of Heat and Fluid Flow*, 27(3):416–423.

Hadi Sichani, P. (2021). Direct numerical simulations of turbulent channel flows at $Re_\tau = 350$. *Unpublished*.

Håkansson, K. M., Kvick, M., Lundell, F., Wittberg, L. P., and Söderberg, L. D. (2013). Measurement of width and intensity of particle streaks in turbulent flows. *Experiments in fluids*, 54(6):1–13.

Heymsfield, A. J. (1977). Precipitation development in stratiform ice clouds: A microphysical and dynamical study. *Journal of Atmospheric Sciences*, 34(2):367–381.

Hoyas, S. and Jiménez, J. (2006). Scaling of the velocity fluctuations in turbulent channels up to Re_τ = 2003. *Physics of fluids*, 18(1):011702.

Hussain, A. K. M. F. and Reynolds, W. C. (1975). Measurements in Fully Developed Turbulent Channel Flow. *Journal of Fluids Engineering*, 97(4):568–578.

Johansson, A. V. and Alfredsson, P. H. (1982). On the structure of turbulent channel flow. *Journal of Fluid Mechanics*, 122:295–314.

Kasagi, N. and Matsunaga, A. (1995). Three-dimensional particle-tracking velocimetry measurement of turbulence statistics and energy budget in a backward-facing step flow. *International Journal of Heat and Fluid Flow*, 16(6):477–485.

Kim, J., Moin, P., and Moser, R. (1987). Turbulence statistics in fully developed channel flow at low reynolds number. *Journal of fluid mechanics*, 177:133–166.

Kind, M. and Martin, H. (2013). *VDI-Wärmeatlas*. Springer.

Kitagawa, A., Hishida, K., and Kodama, Y. (2005). Flow structure of microbubble-laden turbulent channel flow measured by piv combined with the shadow image technique. *Experiments in Fluids*, 38(4):466–475.

Kreplin, H.-P. and Eckelmann, H. (1979). Behavior of the three fluctuating velocity components in the wall region of a turbulent channel flow. *The Physics of Fluids*, 22(7):1233–1239.

Laufer, J. (1948). *Investigation of turbulent flow in a two-dimensional channel*. PhD thesis, California Institute of Technology.

Li, F.-C., Kawaguchi, Y., Segawa, T., and Hishida, K. (2005). Reynolds-number dependence of turbulence structures in a drag-reducing surfactant solution channel flow investigated by particle image velocimetry. *Physics of Fluids*, 17(7):075104.

Lien, K., Monty, J., Chong, M., and Ooi, A. (2004). The entrance length for fully developed turbulent channel flow. In *15th Australian fluid mechanics conference*, volume 15, pages 356–363. University of Sydney, Sydney, Australia.

Lundell, F., Söderberg, L. D., and Alfredsson, P. H. (2011). Fluid mechanics of papermaking. *Annual Review of Fluid Mechanics*, 43:195–217.

Mamori, H., Yamaguchi, K., Sasamori, M., Iwamoto, K., and Murata, A. (2019). Dual-plane stereoscopic piv measurement of vortical structure in turbulent channel flow on sinusoidal riblet surface. *European Journal of Mechanics-B/Fluids*, 74:99–110.

Marusic, I., Monty, J. P., Hultmark, M., and Smits, A. J. (2013). On the logarithmic region in wall turbulence. *Journal of Fluid Mechanics*, 716.

Monty, J. and Chong, M. (2009). Turbulent channel flow: comparison of streamwise velocity data from experiments and direct numerical simulation. *Journal of Fluid Mechanics*, 633.

Moroni, M. and Cenedese, A. (2005). Comparison among feature tracking and more consolidated velocimetry image analysis techniques in a fully developed turbulent channel flow. *Measurement Science and Technology*, 16(11):2307.

Murai, Y., Oishi, Y., Takeda, Y., and Yamamoto, F. (2006). Turbulent shear stress profiles in a bubbly channel flow assessed by particle tracking velocimetry. *Experiments in Fluids*, 41(2):343–352.

Ng, H., Monty, J., Hutchins, N., Chong, M., and Marusic, I. (2011). Comparison of turbulent channel and pipe flows with varying reynolds number. *Experiments in fluids*, 51(5):1261–1281.

Nikuradse, J. (1929). *Untersuchungen über die Strömungen des Wassers in konvergenten und divergenten Kanälen*. VDI-Verlag.

Patel, V. and Head, M. (1969). Some observations on skin friction and velocity profiles in fully developed pipe and channel flows. *Journal of Fluid Mechanics*, 38(1):181–201.

Pope, S. B. (2001). *Turbulent flows*. IOP Publishing.

Rama Reddy, G., Philip, J., and Marusic, I. (2016). The effects of laser-sheet misalignment on stereo-piv measurements in wall-bounded turbulence.

Recktenwald, I., Weller, T., Schröder, W., and Oberlack, M. (2007). Comparison of direct numerical simulations and particle-image velocimetry data of turbulent channel flow rotating about the streamwise axis. *Physics of Fluids*, 19(8):085114.

Reichardt, H. (1938). Messungen turbulenter schwankungen. *Naturwissenschaften*, 26(24):404–408.

Reynolds, O. (1883). Xxix. an experimental investigation of the circumstances which determine whether the motion of water shall be direct or sinuous, and of the law of resistance in parallel channels. *Philosophical Transactions of the Royal society of London*, (174):935–982.

Schaefer, L., Dierksheide, U., Klaas, M., and Schroeder, W. (2011). Investigation of dissipation elements in a fully developed turbulent channel flow by tomographic particle-image velocimetry. *Physics of fluids*, 23(3):035106.

Schanz, D., Gesemann, S., and Schröder, A. (2016). Shake-the-box: Lagrangian particle tracking at high particle image densities. *Experiments in fluids*, 57(5):1–27.

Schultz, M. P. and Flack, K. A. (2013). Reynolds-number scaling of turbulent channel flow. *Physics of Fluids*, 25(2):025104.

So, S., Morikita, H., Takagi, S., and Matsumoto, Y. (2002). Laser doppler velocimetry measurement of turbulent bubbly channel flow. *Experiments in Fluids*, 33(1):135–142.

Vinuesa, R., Bartrons, E., Chiu, D., Dressler, K. M., Rüedi, J.-D., Suzuki, Y., and Nagib, H. M. (2014). New insight into flow development and two dimensionality of turbulent channel flows. *Experiments in fluids*, 55(6):1–14.

Vinuesa, R., Schlatter, P., and Nagib, H. (2018). Secondary flow in turbulent ducts with increasing aspect ratio. *Physical Review Fluids*, 3(5):054606.

Wallace, J. M., Eckelmann, H., and Brodkey, R. S. (1972). The wall region in turbulent shear flow. *Journal of Fluid Mechanics*, 54(1):39–48.

Warholic, M., Heist, D., Katcher, M., and Hanratty, T. (2001). A study with particle-image velocimetry of the influence of drag-reducing polymers on the structure of turbulence. *Experiments in fluids*, 31(5):474–483.

Wei, T. and Willmarth, W. (1989). Reynolds-number effects on the structure of a turbulent channel flow. *Journal of Fluid Mechanics*, 204:57–95.

Wilson, B. M. and Smith, B. L. (2013). Uncertainty on piv mean and fluctuating velocity due to bias and random errors. *Measurement Science and Technology*, 24(3):035302.

Zanoun, E.-S., Durst, F., and Nagib, H. (2003). Evaluating the law of the wall in two-dimensional fully developed turbulent channel flows. *Physics of Fluids*, 15(10):3079–3089.

Zanoun, E.-S., Kito, M., and Egbers, C. (2009a). A study on flow transition and development in circular and rectangular ducts. *Journal of fluids engineering*, 131(6).

Zanoun, E.-S., Nagib, H., and Durst, F. (2009b). Refined cf relation for turbulent channels and consequences for high-re experiments. *Fluid dynamics research*, 41(2):021405.

Zonta, F., Marchioli, C., and Soldati, A. (2012). Modulation of turbulence in forced convection by temperature-dependent viscosity. *Journal of Fluid Mechanics*, 697:150.